

Motion of charged and spinning particles influenced by dark matter field surrounding a charged dyonic black hole

Sanjar Shaymatov,^{1,2,3,4,5,*} Pankaj Sheoran,^{6,†} and Sanjay Siwach^{6,‡}

¹*Institute for Theoretical Physics and Cosmology,
Zhejiang University of Technology, Hangzhou 310023, China*

²*Akfa University, Milliy Bog Street 264, Tashkent 111221, Uzbekistan*

³*Ulugh Beg Astronomical Institute, Astronomicheskaya 33, Tashkent 100052, Uzbekistan*

⁴*National University of Uzbekistan, Tashkent 100174, Uzbekistan*

⁵*Institute of Fundamental and Applied Research,*

National Research University TIIAME, Kori Niyoziy 39, Tashkent 100000, Uzbekistan

⁶*Department of Physics, Institute of Science, Banaras Hindu University, Varanasi-221005, India*

(Dated: June 7, 2022)

We investigate the motion of massive charged and spinning test particles around a charged dyonic black hole surrounded by perfect fluid scalar dark matter field. We obtain the equations of motion and find the expressions for the four-velocity for the case of a charged particle and four-momentum components for the case of a spinning particle. The trajectories for various values of electric Q_e and magnetic Q_m charges are investigated under the influence of dark matter field λ . We study in detail the properties of innermost stable circular orbits (ISCOs) in the equatorial plane. We show that, in addition to the particle's spin, the dark matter field parameter λ and black hole charges (Q_m and Q_e) have a significant influence on the ISCOs of spinning particles. We find that if the spin is parallel to the total angular momentum J (i.e., $S > 0$), the ISCO parameters (i.e., r_{ISCO} , L_{ISCO} , and E_{ISCO}) of a spinning particle are smaller than those of a nonspinning particle, whereas if the spin is antiparallel to total angular momentum J (i.e. $S < 0$), the value of the ISCO parameters is greater than that of the nonspinning particle. We also show that for the corresponding values of spin parameter S , the behavior of Keplerian angular frequency Ω at the ISCO is opposite that of r_{ISCO} , L_{ISCO} , and E_{ISCO} . As an astrophysical application, the study of ISCOs may play a significant role as ISCOs can be used to set the inner edge of the accretion disk around a black hole as well as the initial condition of the binary black hole mergers.

PACS numbers:

I. INTRODUCTION

Black holes have so far been predicted to be formed under gravitational collapse of a sufficiently compact massive object that has exerted all its resources to withstand gravity, and thus they have been very attractive objects with their remarkable geometric properties. Recent observational studies of stellar mass black holes in x-ray binaries and gravitational wave astronomy [1, 2] and supermassive black holes through modern astronomical observations of the Event Horizon Telescope Collaboration and BlackHoleCam [3, 4] have verified the presence of black holes in the Universe. Since much progress has been made in observations of the first image of a supermassive black hole at the center of the M87* galaxy, black holes have been currently considered the main laboratories in testing general relativity and modified theories of gravity. Because of these abovementioned observations, a qualitatively new stage has been opened to study the remarkable gravitational properties of astrophysical black holes and obtain precise constraints and measurement of

black hole parameters.

To understand more deeply and explore the properties of black holes, one needs to investigate the geodesics of test particles and photons as their motion would be a very potent tool in addressing a question in connection with the black hole's nature. In this respect, the test particle trajectories may play a decisive role in understanding the unexplored nature of other existing fields contributing to altering its motion as well as the behavior of background spacetime in the astrophysical context. For example, the motion of test particles gets altered drastically as a consequence of the presence of external magnetic fields [5] and the presence of surrounding matter fields [6, 7]. On the other hand, particle motion around black holes gives the possibility of exhibiting departures of the geometry of astrophysical black holes. There is an extensive body of research involving the effect of the electromagnetic field on the motion of a test particle in the black hole vicinity in various gravity models (, for example [8–15]). Furthermore, one of the other existing matters is the dark matter field that can exist in the environment of supermassive black holes. With this in mind, one is allowed to test the effect of the dark matter field on both the background geometry as well as the test particle motion in a realistic astrophysical context. Regardless of the fact that there is still no direct experimental detection that verifies the presence of dark matter, observations have provided

*Electronic address: sanjar@astrin.uz

†Electronic address: hukmipankaj@gmail.com

‡Electronic address: sksiwach@hotmail.com

strong evidence that dark matter can exist in the environment of giant elliptical and spiral galaxies [16]. Relying on the theoretical analysis and astrophysical data, it is believed that dark matter contributes approximately up to 90 % of the mass of the Galaxy, while the rest is the luminous matter composed of baryonic matter [17]. Astrophysical observations indicate that giant elliptical and spiral galaxies are embedded in a giant dark matter halo [3, 4]. In the literature, there are several black hole solutions that involve the dark matter contribution in the background geometry; here we give the representative ones [18, 19]. Of them, Kiselev derived a static and spherically symmetric black hole with a dark matter profile through a quintessential scalar field [18], according to which the new solution involved a term $\lambda \ln(r/r_q)$ in the metric coefficients. This solution, in turn gave new prosperity in deriving further solutions. Later on, another interesting solution was derived by Li and Yang [19] containing the same term $(r_q/r) \ln(r/r_q)$ represented by a phantom scalar field under the assumption that the dark matter profile is formed from massive particles that must participate in the weak interaction (i.e. weakly interacting massive particles with the equation of state $\omega \simeq 0$). There is a large amount of work that considers the dark matter field in the background spacetime in various situations (see, e.g. [20–27]).

In an astrophysical scenario, black holes can be characterized by at most three parameters, i.e. black hole mass M , rotation a and electric charge Q . Note that the first two parameters are constrained by the black hole mass. Also black holes can be regarded as charged black holes referred to as the Reissner-Nordström black hole solution with mass and electric charge. For example, the detailed analysis of the neutral and charged particle motion around a Reissner-Nordström black hole has been discussed in [28, 29]. There are several astrophysical mechanisms for a black hole to possess charge. A black hole can have a positive net electric charge due to the balance between the Coulomb and gravitational forces for charged particles near the surface of the compact object [30, 31] and due to the matter which gets charged as that of the irradiating photons [32]. It is also worth noting that, by the Wald mechanism [33] the induced charge can be produced by the magnetic field lines getting twisted as that of the frame-dragging effect. However, in all mentioned cases the black hole charge can be regarded as much more weaker (see, for example, [34]). Also, based on the an exact rotating Schwinger dyon solution, a black hole can be endowed with four parameters: mass M , the electric charge Q_e , magnetic charge Q_m , and rotation parameter a [35]. This black hole solution is an interesting case of a charged black hole even if there exists no rotation parameter. In this context, there are several other ways that a black hole can include electric and magnetic charges, and the properties of these black hole solutions have been tested by different astrophysical processes [36, 37].

The analysis of particle motion is a powerful tool to

reveal the geometric properties of compact objects and astrophysical processes in the environment surrounding the black holes [38–43]. In a realistic scenario background spacetime geometry cannot be regarded as vacuum. Thus, in this paper, we consider a charged dyonic black hole placed in the perfect fluid dark matter (PFDM) field. For this spacetime geometry, we study the influence of PFDM on the dynamical motion of magnetically and electrically charged particles moving around this charged dyonic black hole. This may lead us to understand the nature of the gravitational interaction between the charged black hole spacetime and PFDM field. In addition to the motion of a charged particle, we also investigate the motion of a spinning particle moving in the vicinity of a charged dyonic black hole surrounded by a PFDM. For spinning particles, we mainly discuss the properties of innermost stable circular orbit (ISCO) parameters r_{ISCO} , L_{ISCO} , E_{ISCO} , and Ω_{ISCO} and bring out the effect of dark matter field in addition to the black hole charges. The main motivation to study the ISCOs is that they can be treated as the initial condition of the final merger of a binary system of compact objects. Obviously, the motion of a massive test particle is influenced by black hole parameters like charge, mass and spin (see Refs. [44–52]). The study of the ISCOs of the spinning test particle started with the works of Suzuki and Maeda [44] and Jefremov *et al.* [53]. In [44], the ISCOs of a spinning test particle are explored for Kerr a black hole. Later, in [53], the approximate analytical solutions of the ISCOs for a spinning particle are presented for both Schwarzschild and Kerr black holes within the small spin limit. Thereafter, the study of ISCOs for spinning particles in various black hole backgrounds is done [54–63], although, the motion of a spinning particle is studied in various contexts [64–75]. Still, there are not many studies of the ISCOs of a spinning particle when a black hole with the surrounding medium is considered.

Here, we are interested in to seeing how the surrounding medium (say, PFDM in our case) will affect the motion of a spinning particle besides the black hole parameters. It is well known that when the test particle reaction effects (such as self-force corrections) are taken into account, the test particle will follow a nongeodesic trajectory [76–78]. Additionally, if the test particle has a spin due to spin-curvature coupling an extra force is acting on the particle which also results in nongeodesic motion of the spinning test particle [79, 80].

In this paper, we consider only the spin-orbit coupling via “pole-dipole” approximation and discard the reaction of the particle with the black hole background in order to numerically investigate the properties the ISCO of a spinning particle with an arbitrary value of the spin S moving in the charged dyonic black hole immersed in the PFDM. To do so, we use the Tulczyjew spin-supplementary condition (TSSC). We investigate the effect of λ , Q_m , Q_e , and S on the ISCO parameters r_{ISCO} , L_{ISCO} , E_{ISCO} , and Ω_{ISCO} of a spinning test particle together with the superluminal con-

straint (for a brief discussion on the equations of motion of the spinning particle in curved spacetime, TSSC and superluminal constraint, see Appendix A and references therein). It is worth noting that here we are considering the spin orbit coupling only up to first order and discard the higher order spin correction terms known as the $1/c^2$ -approximation (or as quadratic spin corrections) [81, 82].

The paper is organized as follows: In Sec. II, we describe briefly the charged black hole metric which is followed by the study of charged particle dynamics in Sec. III. We investigate the motion of a spinning particle around a charged black hole submerged in a perfect fluid dark matter environment in Sec. IV. In Sec. V, we offer a summary and emphasize the important findings. To make the article self-contained, we include a brief introduction of the Lagrangian theory of the spinning particle in appendix A. In addition, the explicit form of the equations required to identify the ISCOs and the explicit form of the equation expressing the superluminal constraint are provided in appendix B. Throughout this work, we use a system of units in which $G = c = 1$. Greek indices are taken to run from 0 to 3, while latin ones from 1 to 3.

II. THE BLACK HOLE METRIC

We consider the Lagrangian density of Einstein-Maxwell gravity in the presence of the perfect fluid scalar dark matter field [19, 83]

$$\mathcal{S} = \frac{1}{16\pi} \int d^4x \sqrt{-g} \left[R - F_{\mu\nu} F^{\mu\nu} - 2(\nabla_\mu \Phi \nabla^\mu \Phi - 2V(\Phi)) - 4(\mathcal{L}_{DM} + \mathcal{L}_I) \right], \quad (1)$$

with the electromagnetic field tensor

$$F_{\mu\nu} = \partial_\mu A_\nu - \partial_\nu A_\mu + {}^* G_{\mu\nu}, \quad (2)$$

where ${}^* G_{\mu\nu}$ refers to the Dirac string term [83]. Note that $V(\Phi)$ is related to the phantom field potential, while \mathcal{L}_{DM} and \mathcal{L}_I , respectively, refer to the dark matter Lagrangian density and Lagrangian representing the interaction between the dark matter and phantom field. Further \mathcal{L}_I can be regarded as negligible because of small interaction between the phantom field and the dark matter. Let us then write the Einstein field equation for the Einstein-Maxwell gravity in the presence of PFDM,

$$G_{\mu\nu} = R_{\mu\nu} - \frac{1}{2} g_{\mu\nu} R = T_{\mu\nu}, \quad (3)$$

$$\nabla_\mu F^{\mu\nu} = 0, \quad (4)$$

where the energy-momentum tensor $T_{\mu\nu}$ is defined by

$$\begin{aligned} T_{\mu\nu} &= 2F_{\mu\alpha} F_\nu{}^\alpha - \frac{1}{2} g_{\mu\nu} F_{\alpha\beta} F^{\alpha\beta} \\ &\quad + 2\nabla_\mu \Phi \nabla_\nu \Phi - g_{\mu\nu} \nabla_\alpha \Phi \nabla^\alpha \Phi + \\ &\quad + T_{\mu\nu}^{\text{DM}} + T_{\mu\nu}^{\text{I}}, \end{aligned} \quad (5)$$

with $T_{\mu\nu}^{\text{DM}}$ representing the energy-momentum tensor for the PFDM.

We consider the static, spherically symmetric metric ansatz for the black hole as

$$ds^2 = -e^{A(r)} dt^2 + e^{B(r)} dr^2 + r^2 (d\theta^2 + \sin^2 \theta d\phi^2), \quad (6)$$

and then the Einstein equations with Maxwell field can be written in the form [19]

$$e^{-B} \left(\frac{1}{r^2} - \frac{B'}{r} \right) - \frac{1}{r^2} = \frac{Q^2}{r^4} + \frac{1}{2} e^{-B} \Phi'^2 - V(\Phi) - \rho_{\text{DM}}, \quad (7)$$

$$e^{-B} \left(\frac{1}{r^2} + \frac{A'}{r} \right) - \frac{1}{r^2} = \frac{Q^2}{r^4} - \frac{1}{2} e^{-B} \Phi'^2 - V(\Phi), \quad (8)$$

$$e^{-B} \left(A'' + \frac{A'^2}{2} + \frac{A' - B'}{r} - \frac{A'B'}{2} \right) = -\frac{Q^2}{r^4} + \frac{1}{2} e^{-B} \Phi'^2 - V(\Phi). \quad (9)$$

It is worth noting that the components $\theta\theta$ and $\phi\phi$ of the Einstein field equations are identical. From the above Einstein equation, the black hole metric in Boyer-Lindquist coordinates $x^\alpha = (t, r, \theta, \phi)$ is then given by the following line element:

$$ds^2 = -F(r) dt^2 + \frac{dr^2}{F(r)} + r^2 (d\theta^2 + \sin^2 \theta d\phi^2), \quad (10)$$

where $F(r)$ is defined as

$$F(r) = 1 - \frac{2M}{r} + \frac{Q_{e+m}^2}{r^2} + \frac{\lambda}{r} \ln \frac{r}{|\lambda|}, \quad (11)$$

with M being the black hole mass, $Q_{e+m}^2 = Q_e^2 + Q_m^2$ where Q_e and Q_m are the electric and magnetic charges and λ is related to the scale parameter characterized by the PFDM. Thus, the static and spherically symmetric solution black hole can be endowed with three parameters, i.e. mass M , the electric charge Q_e and magnetic charge Q_m . Note that parameters, M , $Q_{e,m}$ and λ are dimensionful quantities, and hence their dimensions are taken to be L^1 having set $G = c = 1$. However, for further analysis we shall for simplicity normalize these parameters as $Q_{e,m}/M$ and λ/M , respectively, in order to define them as dimensionless quantities having set $M = 1$. For $Q_e = Q_m = \lambda = 0$, the black hole spacetime metric surrounded by the PFDM field, i.e., Eq. (10), reduces to the Schwarzschild metric, while for $Q_m = \lambda = 0$ the spacetime metric then reduces to the Reissner-Nordström metric. Similarly, in the case of vanishing Q_e and Q_m , it reduces to the Schwarzschild black hole surrounded by PFDM field. In the case of nonvanishing dark matter distribution, i.e. $\lambda \neq 0$, the energy-momentum tensor for an anisotropic perfect fluid distribution is written as

$$T_\nu^\mu = \text{diag}(-\rho, p_r, p_\theta, p_\phi). \quad (12)$$

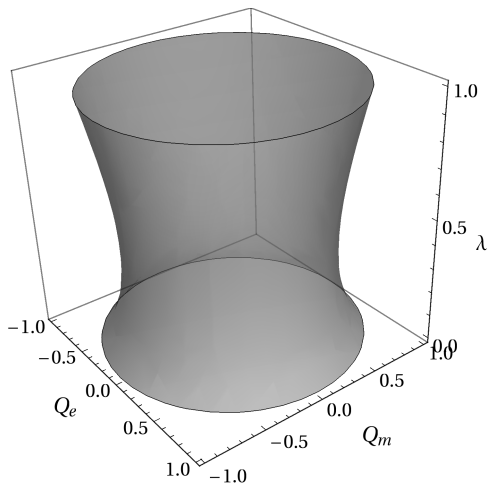


FIG. 1: The limits on the parameters Q_e, Q_m , and λ are presented. The shaded region corresponds to the permitted region for which a black hole exists, while the unfilled region corresponds to the naked singularity.

Here density, radial and tangential pressures will respectively read as

$$\rho = -p_r = \frac{\lambda}{8\pi r^3} \quad \text{and} \quad p_\theta = p_\phi = \frac{\lambda}{16\pi r^3}. \quad (13)$$

We shall only consider the positive value for a dark matter profile $\lambda > 0$ for further analysis, which refers to positive energy density that represents attractive behavior.

The horizon of the black hole is determined as a solution of the following nonlinear equation,

$$1 - \frac{2M}{r} + \frac{Q_{e+m}^2}{r^2} = -\frac{\lambda}{r} \ln \frac{r}{|\lambda|}. \quad (14)$$

In the case of vanishing λ the horizon radius takes the simple form as

$$r_\pm = M \pm \sqrt{M^2 - Q_{e+m}^2}. \quad (15)$$

The above equation corresponds to the outer and inner horizons. If the two outer and inner horizons coincide, i.e. $r_+ = r_-$, it is then interpreted by the extremal charged dyonic black hole for which the following condition is satisfied

$$M^2 = Q_{e+m}^2, \quad (16)$$

while the black hole horizon no longer exists in the case of $M^2 < Q_{e+m}^2$, exhibiting a naked singularity.

In the case of nonvanishing λ , it becomes complicated to solve the nonlinear Eqn. (14) analytically for the black hole horizon. It is, however, possible to reach its analytic form by imposing the condition, i.e., $\lambda \ll M$. In doing

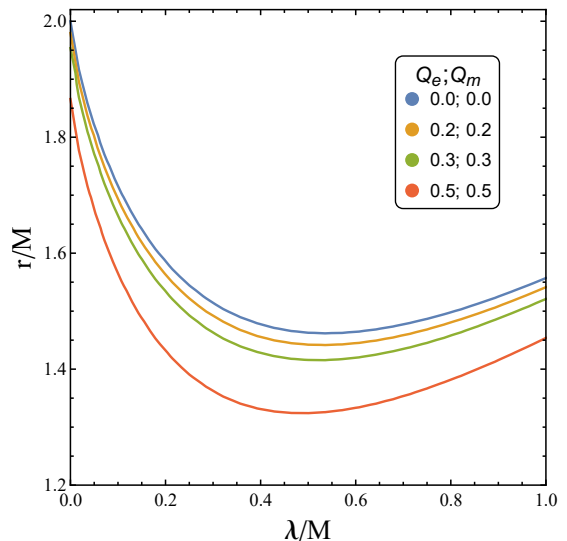


FIG. 2: The horizon radius r_h is plotted as a function of perfect fluid dark matter parameter λ for various values of Q_e and Q_m .

so, one can get the horizon radius in the following form

$$r_\pm = M \pm \left[M^2 - Q_{e+m}^2 - \lambda \left(M + \sqrt{M^2 - Q_{e+m}^2} \right) \times \ln \left(\frac{M + \sqrt{M^2 - Q_{e+m}^2}}{\lambda} \right) \right]^{1/2}. \quad (17)$$

Hereafter, we only use the black hole's outer horizon r_+ popularly known as the event horizon, and use the notation r_h instead of r_+ , unless otherwise specified. In Fig. 1, we show the limits on the parameters Q_e, Q_m , and λ . As can be seen from Fig. 1, the shaded region corresponds to the permitted region for which a black hole exists, while the unfilled region corresponds to the naked singularity. To understand a bit more clearly, in Fig. 2, we show the dependence of the horizon radius r_h on the PFDM parameter λ . From Fig. 2, the black hole horizon radius decreases as parameters Q_e, Q_m , and λ increase till some particular value of λ , and then it starts to grow. This clearly shows that the parameter λ has the physical effect that shifts black hole's outer horizon toward to small r . This is in agreement with the physical meaning of the parameter λ as a repulsive gravitational charge, similarly to the black hole's electric and magnetic charges $Q_{e,m}$. However, it can be seen from Fig. 2 that the radius of the horizon grows in the limit of large λ . This happens because the radial pressure p_r (see, Eqn. (13)) has the repulsive nature, and thus it turns out that the dark matter field, ρ , can be repulsive in the limit of large λ . Hence, we further focus on the small λ in order to manifest more realistic model for the dark matter

distribution.

In the following sections, the motion of magnetically and electrically charged particles, as well as that of neutral spinning particles will be studied. It's worth noting that, we use the Hamiltonian technique to investigate the motion of magnetically and electrically charged particles just because of simplicity. On the other hand to investigate the motion of spinning particle, there are two well-known approaches mainly: the Mathisson-Papapetrou (MP) approach [84, 85] and the Lagrangian approach [79, 86–88]. For the spinning particle, we use the Lagrangian technique rather than the MP approach in this article. The rationale for adopting the Lagrangian approach over the MP approach is explained in appendix A

III. CHARGED PARTICLE DYNAMICS

First, we focus on charged particle motion around a charged black hole in the presence of perfect fluid dark matter. We assume that the test particle is endowed with the rest mass m , electric charge q , and magnetic charge q_m . In general, the Hamilton-Jacobi equation of the system is then expressed as [89]

$$H = g^{\alpha\beta} \left(\frac{\partial S}{\partial x^\alpha} - qA_\alpha + iq_m A_\alpha^* \right) \times \left(\frac{\partial S}{\partial x^\beta} - qA_\beta + iq_m A_\beta^* \right), \quad (18)$$

with the action S with the spacetime coordinates, the components of the vector and the dual vector potentials A_α and A_α^* , and electric and magnetic charges q and q_m . The components of the associated vector potentials A_α and A_α^* of the electromagnetic field take the following form

$$A_\alpha = \left(-\frac{Q_e}{r}, 0, 0, Q_m \cos \theta \right), \\ A_\alpha^* = \left(-\frac{iQ_m}{r}, 0, 0, iQ_e \cos \theta \right). \quad (19)$$

As one can see, the spacetime Eqn. (10) and the components of the vector potential Eqn. (19) are independent of coordinates (t, ϕ) which lead to two conserved quantities, namely, energy E , and angular momentum L of the charged particle measured at infinity. It is known that the Hamiltonian is regarded as a constant $H = k/2$ with relation to $k = -m^2$, where m is the mass of a particle having electric and magnetic charges. Following the Hamilton-Jacobi equation for charged particle motion, we write the action S as follows

$$S = -\frac{1}{2}k\lambda - Et + L\phi + S_r + S_\theta, \quad (20)$$

where S_r and S_θ , respectively, refer to the radial and angular functions of only r and θ . Using Eqn. (20) one

can easily obtain the Hamilton-Jacobi equation in the following form

$$\left(\frac{\partial S_\theta}{\partial \theta} \right)^2 + \left(\frac{L - qQ_m \cos \theta}{\sin \theta} \right)^2 \\ = \frac{r^2}{F} \left(E + \frac{qQ_e}{r} - \frac{q_m Q_m}{r} \right)^2 - r^2 F \left(\frac{\partial S_r}{\partial r} \right)^2 + kr^2. \quad (21)$$

Here one can see that Eqn. (21) is fully separable into radial and angular parts. Hereafter, performing simple algebraic manipulations, one can show that

$$S_r = \int \frac{dr}{F} \sqrt{\left(E + \frac{qQ_e}{r} - \frac{q_m Q_m}{r} \right)^2 - F \left(-k + \frac{K}{r^2} \right)}, \quad (22)$$

$$S_\theta = \int d\theta \sqrt{K - \left(\frac{L - qQ_m \cos \theta}{\sin \theta} \right)^2}, \quad (23)$$

where K is the Carter constant of motion.

From the above equation, E , L , k , and K are independent constants of motion. The fourth one is related to the latitudinal motion and caused by the separability of the action. If we focus on the equatorial motion (i.e., $\theta = \pi/2$) we can further eliminate the fourth constant of motion [89]. We shall for convenience introduce the following notations:

$$\mathcal{E} = \frac{E}{m}, \quad \mathcal{L} = \frac{L}{mM} \quad \text{and} \quad \frac{k}{m^2} = -1. \quad (24)$$

Following Eqns. (21)–(23), we obtain the radial equation of motion for charged particles in the following form

$$\dot{r}^2 = \left(\mathcal{E} - V_{eff(+)}(r) \right) \left(\mathcal{E} - V_{eff(-)}(r) \right), \quad (25)$$

where $V_{eff(\pm)}(r)$ are positive and negative solution of the effective potential $V_{eff}(r)$ describing the radial function of the radial motion and is given by

$$V_{eff(\pm)}(r) = \frac{g_m}{r} - \frac{\sigma_e}{r} \pm \left(1 + \frac{\mathcal{L}^2}{r^2} \right)^{1/2} \\ \times \left(1 - \frac{2M}{r} + \frac{Q_{e+m}^2}{r^2} + \frac{\lambda}{r} \ln \frac{r}{|\lambda|} \right)^{1/2}, \quad (26)$$

where the charge coupling parameters are defined as

$$\sigma_e = \frac{qQ_e}{mM} \quad \text{and} \quad g_m = \frac{q_m Q_m}{mM}, \quad (27)$$

and in further calculations the radial coordinate and dark matter parameter are normalized as $r \rightarrow r/M$ and $\lambda \rightarrow \lambda/M$, respectively. As seen from Eqn. (25), we have either $\mathcal{E} > V_{eff(+)}(r)$ or $\mathcal{E} < V_{eff(-)}(r)$ since $\dot{r}^2 \geq 0$ always. However, we select $V_{eff(+)}(r)$ as an effective potential, i.e. $V_{eff}(r) = V_{eff(+)}(r)$. From Eqn. (26), if we remove all parameters except black hole mass M ,

we can simply recover the effective potential as in the Schwarzschild spacetime. Also, we note that we have written the radial motion for a charged test particle in the equatorial plane (i.e., $\theta = \pi/2$) in the form given by Eqn. (26).

In an astrophysical scenario, it is believed that the environment surrounding black holes cannot be regarded as vacuum as a consequence of the existence of matter and fields. Therefore, it would become increasingly important to take into account the repulsive and attractive effects due to the matter distribution in nearby environment of the black hole. For that we analyze the radial profile of the effective potential $V_{eff}(r)$ that reflects the trajectories of particles for various combinations of charge coupling parameters (σ_e and g_m) and black hole parameters involving black hole charges ($Q_{e,M}$) and dark matter parameter λ that describe the background geometry. As can be seen from Fig. 3, the left panel in the top row reflects the role of σ_e and g_m for the radial profile of the effective potential, while keeping black hole charges Q_e , Q_m fixed and dark matter parameter λ , whereas the right panel reflects the role of parameter λ for the case when parameters Q_e , Q_m , σ_e , and g_m are fixed. The panel in the bottom row of Fig. 3 shows the impact of the parameters Q_e and Q_m on the radial profile of $V_{eff}(r)$ for the case when parameters λ , σ_e and g_m are fixed. From Fig. 3, the height and strength of $V_{eff}(r)$ increase, and its shape shifts toward the event horizon r_h as a consequence of the impact of black hole parameters Q_e , Q_m , and λ . Further, examination of Fig. 3 shows that the inclusion of parameters σ_e and g_m reduces the maximum of $V_{eff}(r)$ and pushes it away from the horizon r_h . Also, one can infer that the combined effect of parameters $Q_{e,m}$ and λ on the profile of the $V_{eff}(r)$ is balanced by the parameters σ_e and g_m . As was stated earlier, we restrict the motion to the equatorial plane, i.e., $\pi = \theta/2$. We then further find a particle trajectory that helps us to understand qualitatively how charged test particle behaves around the black hole under the combined effect of electromagnetic and gravitational forces. In Fig. 4, we show particle trajectory restricted to move on the equatorial plane of the charged dyonic black hole immersed in PFDM. As seen in Fig. 4, there occur for various orbits, i.e. bound, captured and the escaping orbits, depending upon the parameter choices. It is obvious from the particle trajectory that orbits are captured by black hole when the magnetic charge q_m of the particle increases, while they turn the escaping orbits for larger electric charge q_e of the particle. However, it turns out that these orbits become bounded as a consequence of the increase in value of PFDM parameter λ in the case of fixed particle's energy and angular momentum as shown in sub plots of Fig. 4.

Now we turn to the study of the circular orbits of electrically and magnetically charged test particles around the charged dyonic black hole in the presence of PFDM. As we know from the theory of geodesic particles that a test particle needs to satisfy following conditions simul-

taneously in order to move in circular orbits

- the radial velocity should vanish:

$$\frac{dr}{d\tau} = 0 \implies \mathcal{E} = V_{eff}(r). \quad (28)$$

- the radial acceleration should also vanish:

$$\frac{d^2r}{d\tau^2} = 0 \implies \frac{dV_{eff}(r)}{dr} = 0. \quad (29)$$

These two conditions determine the circular orbits both types of circular orbits i.e. stable and unstable.

The above equations lead us to determine the specific angular momentum \mathcal{L} and energy \mathcal{E} for electrically and magnetically charged particles on the circular orbits

$$\mathcal{L}^2 = \frac{2F(r) [r^3 F'(r) + (g_m - \sigma_e)^2] - r^4 F'(r)^2}{(rF'(r) - 2F(r))^2} + \frac{2F(r)\sqrt{4r^2 F(r) - 2r^3 F'(r) + (g_m - \sigma_e)^2}}{(g_m - \sigma_e)^{-1} (rF'(r) - 2F(r))^2}, \quad (30)$$

$$\mathcal{E} = \frac{g_m}{r} - \frac{\sigma_e}{r} + \left(1 + \frac{\mathcal{L}^2}{r^2}\right)^{1/2} \times \left(1 - \frac{2}{r} + \frac{Q_{e+m}^2}{r^2} + \frac{\lambda}{r} \ln \frac{r}{|\lambda|}\right)^{1/2}, \quad (31)$$

where ' refers to a derivative with respect to r . It is worth noting that in the case $g_m = \sigma_e$, we obtain \mathcal{L} for the Reissner-Nordström black hole case. We now analyze the radial profiles of the specific angular momentum for charged particles so as to understand the behavior of the circular orbits around the black hole. In Fig. 5, we show the radial profile of the specific angular momentum \mathcal{L} for charged particles at the circular orbits around a charged dyonic black hole immersed in PFDM. As shown in Fig. 5, the left panel reflects the impact of the charge coupling parameters g_m and q_e on the radial profile of \mathcal{L} for fixed values of black hole charges Q_e and Q_m and PFDM parameter λ , while the right panel reflects the impact of the dark matter while keeping the black hole charge and charge coupling parameters fixed. From Fig. 5, one can easily see that circular orbits of electrically and magnetically charged particles move at larger radii as we increase the charge coupling parameters g_m and σ_e (see left panel) In contrast, circular orbits move toward smaller radii and become close to the black hole horizon r_h with increasing PFDM parameter λ . Additionally, what we observe from the above analysis is that both black hole charges $Q_{e,m}$ and PFDM parameter λ bring the radii of the circular orbits closer to the r_h of the black hole, thus behaving as a repulsive nature as a result

On the other hand, another limit of the existence of circular orbits is described by the radius for unstable circular photon orbits r_{ph} , which is determined by the divergence of either the specific angular momentum \mathcal{L} or

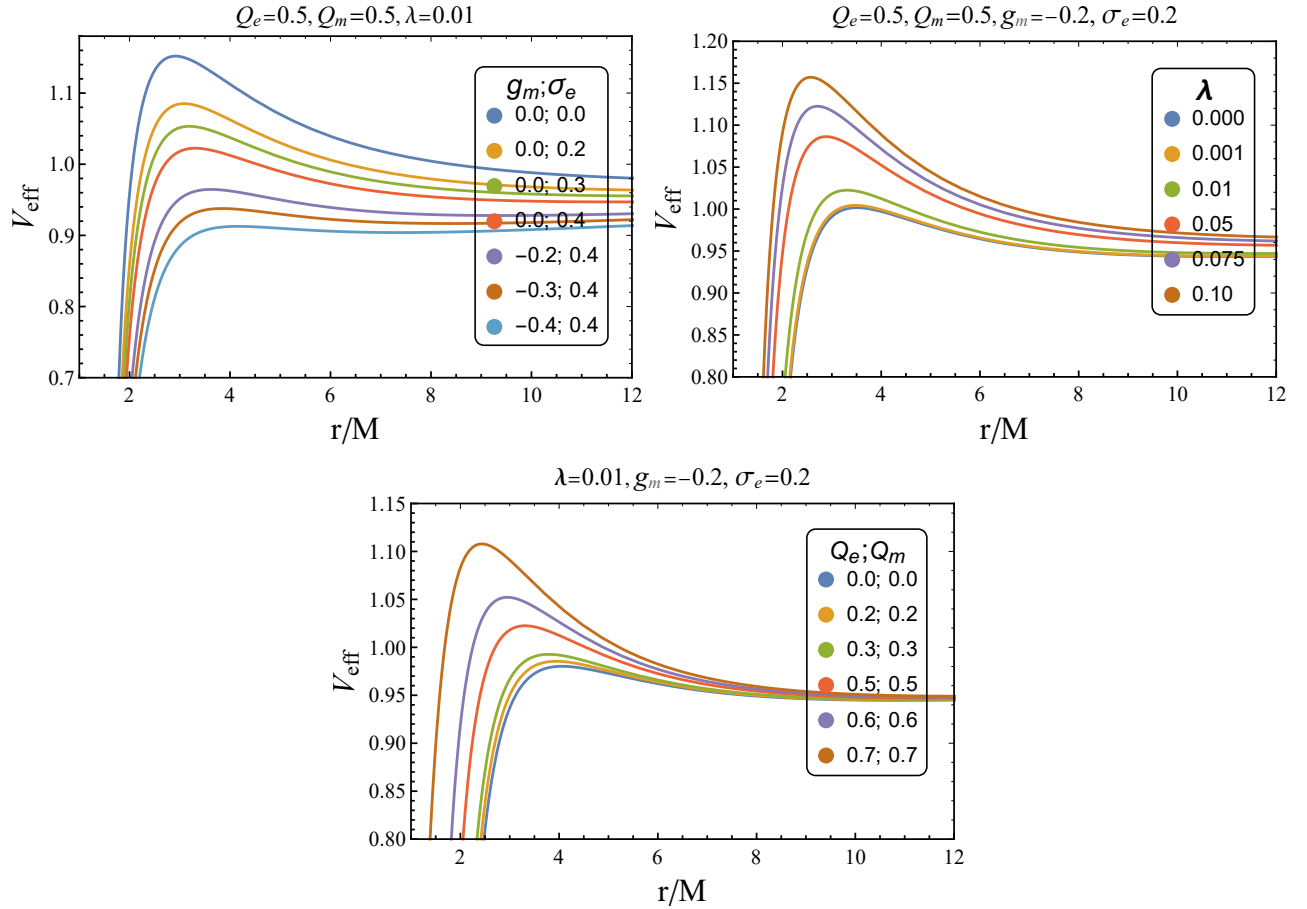


FIG. 3: Radial profile of the effective potential V_{eff} as a function of the spatial distance r/M for massive charged particles orbiting an electrically and magnetically charged black hole immersed in PFDM field. Top row, left panel: V_{eff} is plotted for different values of the charge coupling parameters g_m and σ_e . Top row, right panel: V_{eff} is plotted for different values of dark matter parameter λ . The panel in the bottom row shows V_{eff} versus r/M for different values of black hole electric Q_e and magnetic charge Q_m while keeping fixed the dark matter parameter λ and the charge coupling parameters g_m and σ_e .

energy \mathcal{E} . From Eqns. (30)–(31), one can easily obtain the limit on the existence of circular orbits that always exist at $r > r_{ph}$,

$$rF'(r) - 2F(r) = 0, \quad (32)$$

which gives the radii of the photon orbits. We shall, for simplicity, consider $\lambda \ll 1$ to determine the approximate expression for the photon orbit r_{ph} as

$$\begin{aligned} r_{ph} \approx & \frac{1}{2} \left(3M + \left[9M^2 - 8Q_{e+m}^2 \right. \right. \\ & + \lambda \left(3M + \sqrt{9M^2 - 8Q_{e+m}^2} \right) \\ & - 3\lambda \left(3M + \sqrt{9M^2 - 8Q_{e+m}^2} \right) \\ & \left. \left. \times \ln \left(\frac{3M + \sqrt{9M^2 - 8Q_{e+m}^2}}{2\lambda} \right) \right]^{1/2} \right) \\ & + O(\lambda^2). \end{aligned} \quad (33)$$

From the above expression one can easily see that it explicitly reduces to the Schwarzschild case, i.e., $r_{ph} = 3$ in the limit $\lambda, Q_{e,m} \rightarrow 0$. However, it is certain from Eqn. (33) that r_{ph} decreases as we increase both the parameters λ and $Q_{e,m}$.

Next, in order to determine the ISCO we need to find limiting value of orbital angular momentum \mathcal{L} for which $V_{eff}(r)$ still has an extremum. The ISCO lies at the position where the maximum and minimum of effective potential $V_{eff}(r)$ merge. Hence, one more condition is needed beside conditions Eqns. (28)–(29), which reads

- the second derivative of $V_{eff}(r)$ with respect to radial coordinate r should vanish:

$$\frac{d^2 V_{eff}(r)}{dr^2} = 0. \quad (34)$$

For being somewhat more quantitative, in Table I we show the numerical values of ISCO parameters \mathcal{L}_{ISCO} , \mathcal{E}_{ISCO} and r_{ISCO} for various combinations of $Q_{e,m}$, σ_e , g_m and λ . As shown in Table I both $Q_{e,m}$ and

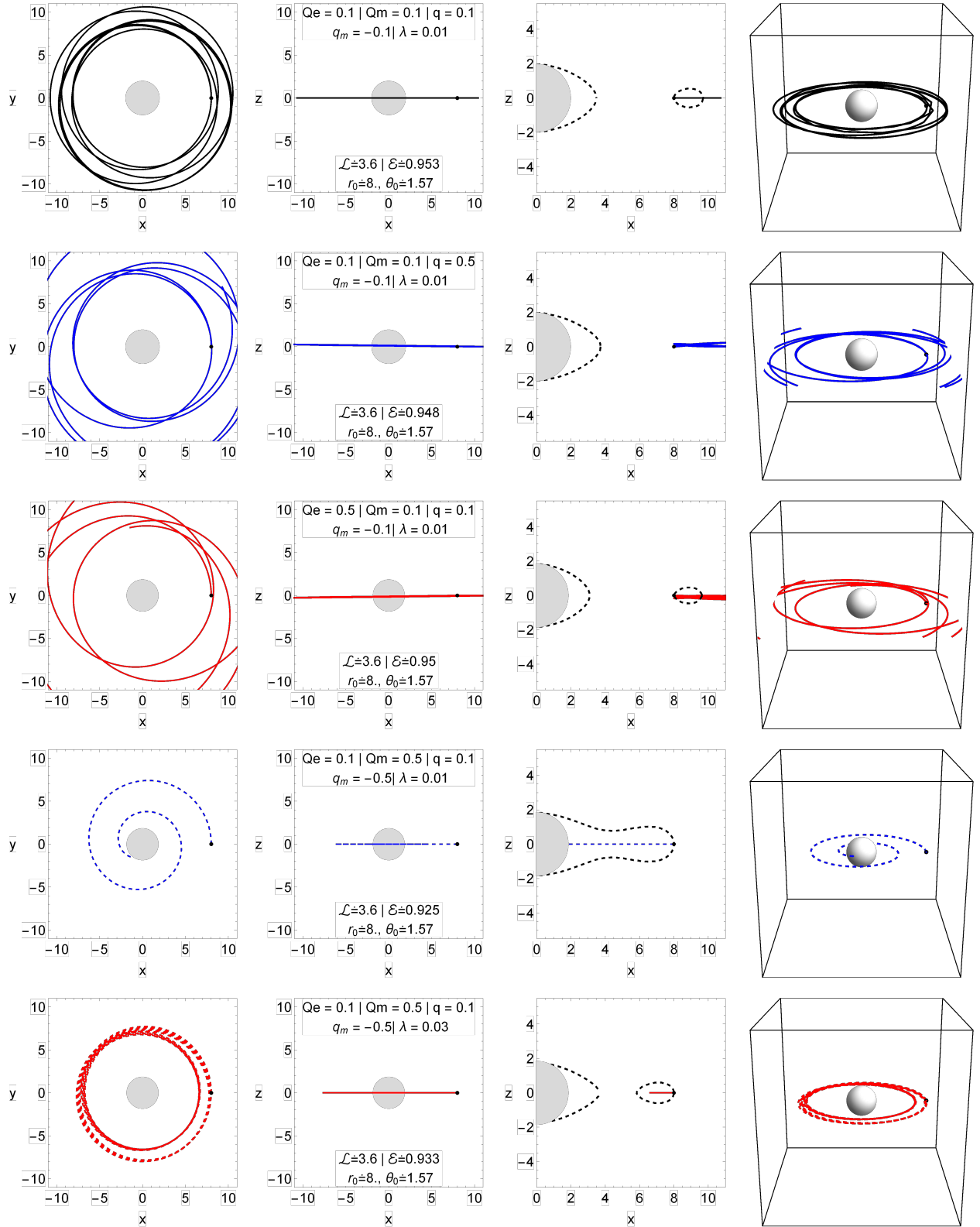


FIG. 4: 2D and 3D trajectories of the charged particles observed from the polar view (i.e., $z = 0$; see the first column) and from the equatorial view (i.e., $y = 0$; see the second column), as well as the boundaries of the motion of charged particles observed from the equatorial view (i.e., $y = 0$; see the third column) around an electrically and magnetically charged dyonic black hole surrounded by PFDM field for various possible cases.

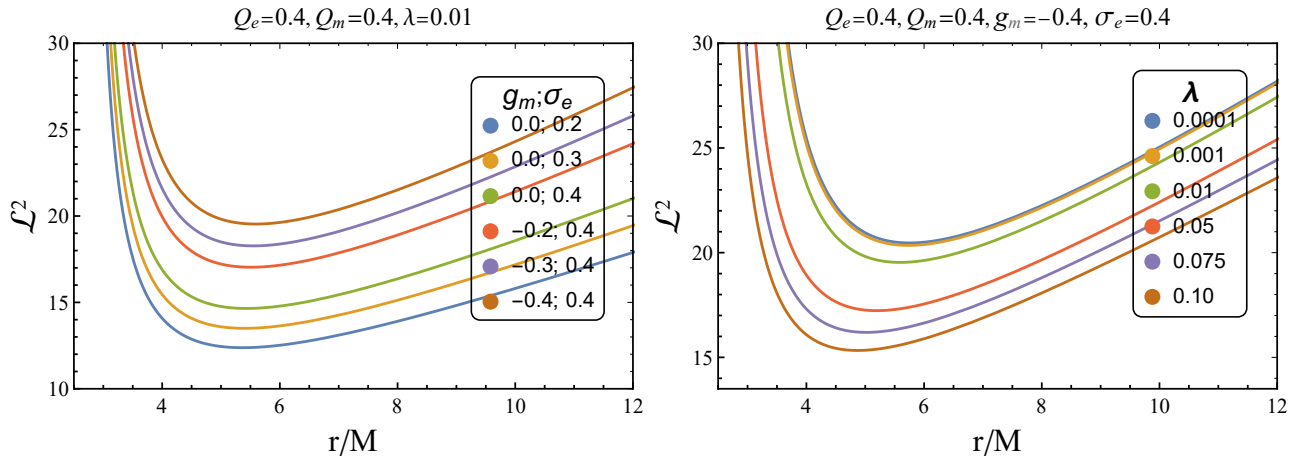


FIG. 5: Radial profile of the specific angular momentum \mathcal{L} as a function of the spatial distance r/M for massive charged particles orbiting a charged dyonic black hole immersed in PFDM field. Left panel: \mathcal{L}^2 is plotted for different values of charge coupling parameters g_m and σ_e while keeping the PFDM parameter λ and Q_e and Q_m fixed. Right panel: \mathcal{L}^2 is plotted for different values of PFDM parameter λ while keeping the rest of the parameters fixed as shown in the plot.

λ have similar effect that decreases the r_{ISCO} . However, the r_{ISCO} increases as a consequence of the increasing the charge coupling parameters g_m and σ_e . Furthermore, one can see that the combined effect of both $Q_{e,m}$ and λ respectively decreases \mathcal{L}_{ISCO} and increases \mathcal{E}_{ISCO} , while the opposite is the case as we increase the charge coupling parameters, as seen in Table I.

Let us then consider the orbital and angular velocity of an electrically and magnetically charged particle moving around the charged dyonic black hole surrounded by PFDM, measured by a local observer [89, 90]. For that, we first write the coordinate velocity components for the particles:

$$v_{\hat{r}} = \sqrt{-\frac{g_{rr}}{g_{tt}} \frac{dr}{dt}} = \sqrt{1 - F \frac{r^2 + \mathcal{K}}{(r\mathcal{E} + \sigma_e - g_m)^2}}, \quad (35)$$

$$v_{\hat{\theta}} = \sqrt{-\frac{g_{\theta\theta}}{g_{tt}} \frac{d\theta}{dt}} = \frac{\sqrt{F}}{r\mathcal{E} + \sigma_e - g_m} \sqrt{\mathcal{K} - \left(\frac{\mathcal{L} - \sigma_m \cos \theta}{\sin \theta}\right)^2}, \quad (36)$$

$$v_{\hat{\phi}} = \sqrt{-\frac{g_{\phi\phi}}{g_{tt}} \frac{d\phi}{dt}} = \frac{\sqrt{F}}{r\mathcal{E} + \sigma_e - g_m} \frac{\mathcal{L} - \sigma_m \cos \theta}{\sin \theta}, \quad (37)$$

where the Carter constant parameter \mathcal{K} becomes irrelevant when we restrict motion to the equatorial plane, i.e., $\theta = \pi/2$. For the particle energy, its classical form can be written as follows:

$$\mathcal{E} = \frac{\sqrt{F}}{\sqrt{1 - v^2}} - \frac{\sigma_e}{r} + \frac{g_m}{r}, \quad (38)$$

where $v = \left(v_{\hat{r}}^2 + v_{\hat{\theta}}^2 + v_{\hat{\phi}}^2\right)^{1/2}$ and we have defined $v = v/c$. As can be easily seen from Eqs. (35-37) $v_{\hat{\theta}} = v_{\hat{\phi}} = 0$ always, while the radial velocity is given by $v_{\hat{r}} = 1$ very near the black hole horizon, i.e. $F(r) = 0$. Similarly, one

can determine the particle linear velocity at the ISCO radius (see, for example [28]). The radial and latitudinal velocities vanish, i.e. $v_r = v_\theta = 0$ at the ISCO, yet the particle orbital velocity takes the form

$$v_\phi = \sqrt{\frac{\partial_r g_{tt}}{\partial_r g_{\phi\phi}} \frac{g_{\phi\phi}}{g_{tt}}}, \quad (39)$$

where $\Omega = \sqrt{-\partial_r g_{tt} / \partial_r g_{\phi\phi}}$ corresponds to the orbital angular velocity of test particle, i.e., the so-called Keplerian angular frequency. Equation (39) then yields

$$v = \sqrt{\frac{1}{2} \left[\frac{r(\lambda + r) - Q_e^2 - Q_m^2}{r(r - 2M) + Q_e^2 + Q_m^2 + \lambda r \ln \frac{r}{|\lambda|}} - 1 \right]}. \quad (40)$$

It is worth noting here that the v_{ISCO} for the Schwarzschild black hole (i.e. $v_{ISCO} = 1/2$) may be readily recovered from the preceding equation when the black hole parameters $Q_{e,m}$ and λ both disappear simultaneously.

We now analyze the radial profile of orbital velocity v for a test particle at ISCO in order to have detailed information about the background geometry of the charged dyonic black hole surrounded by PFDM as compared to the one for the Schwarzschild black hole case. In Fig. 6, we show the radial profile of the orbital velocity v for test particles orbiting at the ISCO radius. From Fig. 6, one can easily see that the orbital velocity of test particle around a charged dyonic black hole immersed in PFDM decreases, and its shape shifts down to smaller v as a consequence of an increase in the value of both black hole charges, i.e., Q_e and Q_m and PFDM parameter λ . However, this may not be the case in general. Thus, we need to explore it numerically to understand the behavior of the orbital velocity better. The behavior of the results on the orbital velocity demonstrated in Fig. 6, is explained

TABLE I: Numerical values of the ISCO parameters \mathcal{L}_{ISCO} , \mathcal{E}_{ISCO} , r_{ISCO} , v_{ISCO} and Ω_{ISCO} of the test particles orbiting on the ISCO around the charged dyonic black hole surrounded by PFDM field are tabulated for various possible cases.

λ	$Q_e/Q_m = 0.0/0.0 \mid \sigma_e/g_m = 0.0/0.0$					$Q_e/Q_m = 0.4/0.0 \mid \sigma_e/g_m = 0.0/0.0$					$Q_e/Q_m = 0.4/0.0 \mid \sigma_e/g_m = 0.2/0.0$				
	\mathcal{L}_{ISCO}	\mathcal{E}_{ISCO}	r_{ISCO}	v_{ISCO}	Ω_{ISCO}	\mathcal{L}_{ISCO}	\mathcal{E}_{ISCO}	r_{ISCO}	v_{ISCO}	Ω_{ISCO}	\mathcal{L}_{ISCO}	\mathcal{E}_{ISCO}	r_{ISCO}	v_{ISCO}	Ω_{ISCO}
0.00001	3.46388	0.94280	5.99964	0.49999	0.06804	3.38450	0.94056	5.75241	0.50710	0.07146	3.70498	0.92948	5.78308	0.50510	0.07090
0.0001	3.46231	0.94281	5.99709	0.49998	0.06807	3.38289	0.94057	5.74975	0.50709	0.07149	3.70337	0.92949	5.78043	0.50509	0.07093
0.001	3.45019	0.94288	5.97791	0.49987	0.06828	3.37054	0.94063	5.72974	0.50703	0.07174	3.69097	0.92950	5.76035	0.50503	0.07117
0.01	3.36533	0.94361	5.84896	0.49871	0.06973	3.28414	0.94127	5.59512	0.50620	0.07344	3.60415	0.92986	5.62457	0.50423	0.07287
0.1	2.89896	0.95197	5.22562	0.48511	0.07727	2.81143	0.94926	4.94006	0.49461	0.08260	3.12739	0.93595	4.94999	0.49386	0.08235
0.2	2.60524	0.96260	4.93536	0.46682	0.08052	2.51714	0.95991	4.62883	0.47773	0.08703	2.82894	0.94510	4.60552	0.47959	0.08771
λ	$Q_e/Q_m = 0.4/0.4 \mid \sigma_e/g_m = 0.2/-0.2$					$Q_e/Q_m = 0.4/0.4 \mid \sigma_e/g_m = 0.4/-0.4$					$Q_e/Q_m = 0.4/0.4 \mid \sigma_e/g_m = 0.6/-0.6$				
	\mathcal{L}_{ISCO}	\mathcal{E}_{ISCO}	r_{ISCO}	v_{ISCO}	Ω_{ISCO}	\mathcal{L}_{ISCO}	\mathcal{E}_{ISCO}	r_{ISCO}	v_{ISCO}	Ω_{ISCO}	\mathcal{L}_{ISCO}	\mathcal{E}_{ISCO}	r_{ISCO}	v_{ISCO}	Ω_{ISCO}
0.00001	3.93127	0.91596	5.59874	0.50781	0.07329	4.52552	0.89618	5.75601	0.49774	0.07036	5.09500	0.87829	5.93189	0.48716	0.06732
0.0001	3.92961	0.91595	5.59599	0.50780	0.07333	4.52384	0.89616	5.75328	0.49773	0.07040	5.09329	0.87825	5.92918	0.48715	0.06735
0.001	3.91685	0.91591	5.57510	0.50776	0.07360	4.51089	0.89605	5.73257	0.49764	0.07065	5.08012	0.87811	5.90859	0.48702	0.06757
0.01	3.82753	0.91584	5.43343	0.50720	0.07551	4.41997	0.89552	5.59141	0.49680	0.07239	4.98741	0.87719	5.76778	0.48591	0.06915
0.1	3.33649	0.91936	4.71908	0.49886	0.08667	3.91536	0.89583	4.86898	0.48756	0.08272	4.46823	0.87485	5.03933	0.47559	0.07859
0.2	3.02976	0.92671	4.34079	0.48696	0.09372	3.59461	0.90046	4.47181	0.47621	0.08958	4.13293	0.87719	4.62913	0.46415	0.08499

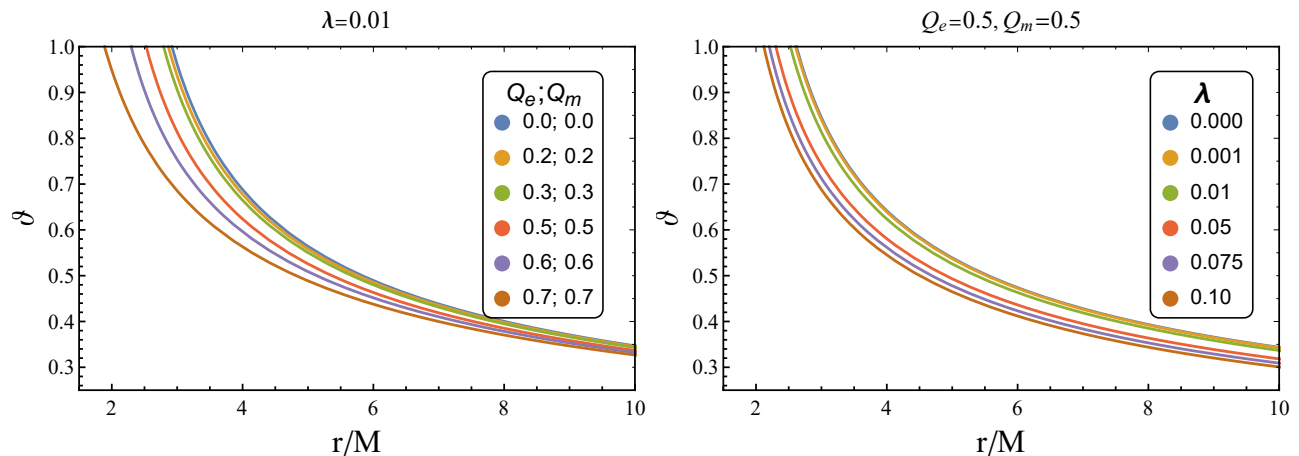


FIG. 6: Radial profile of the orbital velocity v as a function of the spatial distance r/M for test particles orbiting a black hole surrounded by PFDM field. Left panel: v is plotted for different combinations of black hole parameters Q_e and Q_m while keeping the PFDM parameter λ fixed. Right panel: v is plotted for different values of PFDM parameter λ while keeping the black hole charge parameters Q_e and Q_m fixed.

in detail in Table I. From Table I, one can infer that the orbital velocity v decreases when increasing the PFDM parameter λ , while it increases due to the effect of black hole charges Q_e and Q_m .

IV. SPINNING PARTICLE DYNAMICS

In this section, we focus on the study of motion of a spinning particle moving around a charged dyonic black hole in the presence of PFDM. Corinaldesi and Papapetrou [91] first studied the motion of a spinning particle moving in the vicinity of a Schwarzschild black hole. Later, Hojman [86] used the Lagrangian approach to find the equation of motion for the spinning particles. In this section, we use the Lagrangian approach to study the motion of a spinning particle (for a thorough explanation of why we chose the Lagrangian approach over the Mathisson [84] and Papapetrou [85] approach, (see appendix A)).

We start by describing the Killing vectors for the met-

ric of a charged dyonic black hole immersed in PFDM

$$\begin{aligned}
 \zeta_\mu^0 &= (-F(r), 0, 0, 0), \\
 \zeta_\mu^1 &= (0, 0, 0, r^2 \sin^2 \theta), \\
 \zeta_\mu^2 &= (0, 0, r^2 \sin \phi, r^2 \cos \theta \cos \phi \sin \theta), \\
 \zeta_\mu^3 &= (0, 0, r^2 \cos \phi, -r^2 \cos \theta \sin \phi \sin \theta). \quad (41)
 \end{aligned}$$

As the metric (10) is independent of time, we can find the four constants of motion via a simple calculation using the above Killing vectors. For simplicity we are focusing only on the spinning particle motion in the equatorial (i.e., $\theta = \pi/2$) plane. First, we find the constant of motion (i.e., conserved energy E and total angular momentum J perpendicular to the $\theta = \pi/2$ plane) for the spinning particle using the Killing vectors and Eqn. (A13)

$$E = F(r)P^t - \frac{1}{2}S^{tr}F(r)', \quad (42)$$

$$J = r^2 P^\phi + r S^{r\phi}, \quad (43)$$

where the symbol ($'$) represents the derivative with respect to radial coordinate “ r ”. Using the conservation

Eqns. (A6) and (A7), we find another two constants of motion (i.e., mass and spin):

$$m^2 = F(r) (P^t)^2 - \frac{(P^r)^2}{F(r)} - r^2 (P^\phi)^2, \quad (44)$$

$$S^2 = - (S^{tr})^2 + \frac{r^2}{F(r)} (S^{r\phi})^2 - r^2 F(r) (S^{t\phi})^2. \quad (45)$$

On the other hand, the TSSC Eqn. (A8) for our case

reads

$$\frac{S^{tr} P^r}{F(r)} + r^2 S^{t\phi} P^\phi = 0, \quad (46)$$

$$F(r) S^{tr} P^t + r^2 S^{r\phi} P^\phi = 0, \quad (47)$$

$$F(r) S^{t\phi} P^t - \frac{S^{r\phi} P^r}{F(r)} = 0. \quad (48)$$

The four-momentum Eqn. (A4) for the metric (10) reduces to the following equations:

$$\dot{P}^t + \frac{F'(r)\dot{r}}{2F(r)} P^t + \frac{F'(r)}{2F(r)} P^r = \frac{F''(r)\dot{r}}{2F(r)} S^{tr} + \frac{rF'(r)\dot{\phi}}{2} S^{t\phi}, \quad (49)$$

$$\dot{P}^r + \frac{F(r)F'(r)}{2} P^t - \frac{F'(r)\dot{r}}{2F(r)} P^r - rF(r)\dot{\phi} P^\phi = \frac{F(r)F''(r)}{2} S^{tr} + \frac{rF'(r)\dot{\phi}}{2} S^{r\phi}, \quad (50)$$

$$\dot{P}^\phi + \frac{\dot{r}}{r} P^\phi + \frac{\dot{\phi}}{r} P^r = \frac{F(r)F'(r)}{2r} S^{t\phi} - \frac{F'(r)\dot{r}}{2rF(r)} S^{r\phi}, \quad (51)$$

and the equations of motion for the spin calculated from Eqn. (A5) turn out to be

$$\dot{S}^{tr} - rF(r)\dot{\phi} S^{t\phi} = \dot{r} P^t - P^r, \quad (52)$$

$$\dot{S}^{t\phi} + \frac{F'(r)}{2F(r)} S^{r\phi} + \dot{r} \left(\frac{F'(r)}{2F(r)} + \frac{1}{r} \right) S^{t\phi} + \frac{\dot{\phi}}{r} S^{tr} = \dot{\phi} P^t - P^\phi, \quad (53)$$

$$\dot{S}^{r\phi} + \frac{F(r)F'(r)}{2} S^{t\phi} + \dot{r} \left(\frac{1}{r} - \frac{F'(r)}{2F(r)} \right) S^{r\phi} = \dot{\phi} P^r - \dot{r} P^\phi. \quad (54)$$

where the over-dot sign ($\dot{}$) indicates the derivative with respect to coordinate time. Using these 13 equations [i.e., Eqns. (42)–(54)], one can completely determine the motion of a spinning particle in vicinity of a charged dyonic black hole in PFDM. Using Eqns. (46) and (47), one can write

$$\left[F(r)(P^t)^2 - \frac{(P^r)^2}{F(r)} \right] (S^{tr})^2 = r^4 \left[\frac{(S^{r\phi})^2}{F(r)} - F(r)(S^{t\phi})^2 \right] (P^\phi)^2. \quad (55)$$

Now, using conservation of mass and spin Eqns. (44) and (45) together with Eqn. (55), the expression for S^{tr} comes out as

$$S^{tr} = \pm \frac{rSP^\phi}{m}. \quad (56)$$

Using Eqns. (42), (43) and (47), the relation between the conserved E and J is

$$\left(E + \frac{S^{tr}F'(r)}{2} \right) S^{tr} + (J - r^2 P^\phi) r P^\phi = 0, \quad (57)$$

which can be solved explicitly for P^ϕ after substituting the value of S^{tr} from Eqn. (56). The expression for P^ϕ reads as

$$\frac{P^\phi}{m} = \frac{2r^2 (\mathcal{J} - \mathcal{S}\mathcal{E})}{2r^4 + 2Q_{e+m}^2 S^2 - (2M + \lambda) r S^2 + r S^2 \lambda \ln \frac{r}{|\lambda|}}, \quad (58)$$

where $Q_{e+m}^2 = Q_e^2 + Q_m^2$, and $\mathcal{J} = J/m$, $\mathcal{S} = \mp S/m$ and $\mathcal{E} = E/m$ are the total angular momentum, spin and energy per unit mass, respectively. Here, \mathcal{S} (negative) positive means that the spin of the particle is (anti-) parallel to J . It is important to note here that total angular momentum per unit mass \mathcal{J} is equal to the sum of spin angular momentum per unit mass f and orbital angular momentum per unit mass L . Similarly, using Eqns. (42), (56) and (58), we find the time component of the four-momentum

$$\frac{F(r)P^t}{m} = \frac{2r^4 \mathcal{E} + \left[Q_{e+m}^2 - 2Mr - r\lambda + r\lambda \ln \frac{r}{|\lambda|} \right] \mathcal{J}\mathcal{S}}{2r^4 + 2Q_{e+m}^2 S^2 - (2M + \lambda) r S^2 + r S^2 \lambda \ln \frac{r}{|\lambda|}}, \quad (59)$$

which further leads to the explicit expression of P^r by using Eqn. (58) and conservation of mass Eqn. (44)

$$\frac{(Pr)^2}{m^2} = \left(\frac{2r^4 \mathcal{E} + [Q_{e+m}^2 - 2Mr - r\lambda + r\lambda \ln \frac{r}{|\lambda|}] \mathcal{J}\mathcal{S}}{2r^4 + 2Q_{e+m}^2 S^2 - (2M + \lambda) r S^2 + r S^2 \lambda \ln \frac{r}{|\lambda|}} \right)^2 - F(r) - \left(\frac{2r^3 \sqrt{F(r)} (\mathcal{J} - \mathcal{S}\mathcal{E})}{2r^4 + 2Q_{e+m}^2 S^2 - (2M + \lambda) r S^2 + r S^2 \lambda \ln \frac{r}{|\lambda|}} \right)^2. \quad (60)$$

It is worth noting here that in the limits $\mathcal{S} \rightarrow 0$ and $\lambda \rightarrow 0$, the Eqns. (58)–(60) reduce to the nonzero components of the four-momentum for the Schwarzschild black hole obtained in [92].

Next, we are interested in the explicit form of the radial and azimuthal components of coordinate velocity (i.e., \dot{r} and $\dot{\phi}$), since they will help us later to confine the motion of the spin particle to the subluminal zone, which is the region where the particle's four-velocity is timelike. With this aim in mind, we need to first find the unknown components of the spin tensor (i.e., $S^{t\phi}$ and $S^{r\phi}$) in terms of known four-momentum components. By using the first [Eqn. (46)] and second [Eqn. (47)] TSSC together with Eqn. (56) it is easy to show that the components $S^{t\phi}$ and $S^{r\phi}$ of the spin tensor can be written as

$$S^{t\phi} = \frac{\mathcal{S}P^r}{rF(r)} \quad (61)$$

and

$$S^{r\phi} = \frac{\mathcal{S}F(r)P^t}{r}. \quad (62)$$

To determine \dot{r} first, we multiply the factor $\pm(\mathcal{S}r)$ to the TSSC Eqn. (48) and subtract Eqn. (52) together with the help of Eqns. (61) and (62), we get

$$-\dot{S}^{tr} + \mathcal{S}P^r \dot{\phi} = -\dot{r}P^t + P^r \quad (63)$$

This, when combined with Eqns. (51) and (56) along with Eqns. (61) and (62), allows us to find the precise symbolic expression as

$$\dot{r} \equiv \frac{dr}{dt} = \frac{P^r}{P^t}, \quad (64)$$

and now, to calculate $\dot{\phi}$, we utilize Eqns. (56), (58), (61) and (64) in Eqn. (52). With a little algebra, we obtain

$$\dot{\phi} \equiv \frac{d\phi}{dt} = \left[\frac{2 - F''(r)S^2}{2 \left(1 - \frac{F'(r)S^2}{2r} \right)} \right] \frac{P^\phi}{P^t}. \quad (65)$$

It is also observed that the spatial component of the spin perpendicular to the $\theta = \pi/2$ plane is

$$\begin{aligned} S_z &= rS^{r\phi}, \\ &= m\mathcal{S} \left(\frac{2r^4 \mathcal{E} + [Q_{e+m}^2 - 2Mr - r\lambda + r\lambda \ln \frac{r}{|\lambda|}] \mathcal{J}\mathcal{S}}{2r^4 + 2Q_{e+m}^2 S^2 - (2M + \lambda) r S^2 + r S^2 \lambda \ln \frac{r}{|\lambda|}} \right), \end{aligned} \quad (66)$$

which in the asymptotic limit (i.e., $r \rightarrow \infty$) becomes $S_z/m = \mathcal{S}\mathcal{E}$. It is also worth mentioning that, as demonstrated in [92, 93], one may simply bypass the four-momentum and four-velocity relation Eqn. (A12) and work with coordinate velocities solely in the case of static spherically symmetric spacetimes. As a result, we directly found the necessary coordinate velocities in Eqns. (64) and (65) (i.e. \dot{r} and $\dot{\phi}$, respectively) instead of the four-velocity of the spinning particle.

A. Effective potential

It is well known from Newtonian mechanics that the equations of motion can be solved in terms of the radial coordinate [94] to study the motion of a test particle in a central force field, and that in general relativity, the ‘‘effective potential’’ method is widely used to study the dynamics of a test particle in the black hole background.

Because the radial velocity u^r is parallel to the radial component P^r of the four-momentum P^μ [53], the effective potential V_{eff} of the spinning particle moving in the background of a charged dyonic black hole in PFDM can be computed using the P^r Eqn. (60). Since this equation is quadratic in \mathcal{E} , factorizing it separates the energy component from the radial component, giving us

$$\frac{(P^r)^2}{m^2} = \mathcal{A}\mathcal{B}^{-2} [\mathcal{E} - V_{eff(+)}(r)] [\mathcal{E} - V_{eff(-)}(r)], \quad (67)$$

where, \mathcal{A}, \mathcal{B} and the $V_{eff(\pm)}$ are

$$V_{eff(\pm)}(r) \equiv V_{eff(\pm)} = \frac{\mathcal{C} \pm \sqrt{\mathcal{D}}}{2\mathcal{A}}, \quad (68)$$

were defined, with

$$\mathcal{A} \equiv 1 + \frac{\mathcal{S}^2 \mathcal{X}}{r^4}, \quad \mathcal{B} \equiv 1 + \frac{\mathcal{S}^2 \mathcal{Y}}{2r^4}, \quad (69)$$

$$\mathcal{C} \equiv -\frac{\mathcal{J}\mathcal{S}}{r^4} (\mathcal{Y} - 2\mathcal{X}), \quad (70)$$

$$\begin{aligned} \mathcal{D} &\equiv \left(\frac{\mathcal{J}\mathcal{S}}{r^2} \right)^2 \left(\frac{\mathcal{Y} - 2\mathcal{X}}{r^2} \right)^2 - \mathcal{A} \left[4\mathcal{J}^2 \mathcal{X} \right. \\ &\quad \left. + \left(\frac{\mathcal{J}\mathcal{S}\mathcal{Y}}{r^2} \right)^2 + 2\mathcal{X}r^2 \mathcal{B}^2 \right], \end{aligned} \quad (71)$$

$$\mathcal{X} \equiv -\lambda r \ln \frac{r}{|\lambda|} + 2Mr - Q_{e+m}^2 - r^2, \quad (72)$$

$$\mathcal{Y} \equiv \lambda r \ln \frac{r}{|\lambda|} - 2Mr + 2Q_{e+m}^2 - \lambda r. \quad (73)$$

TABLE II: Numerical values of radial component r and bound on spin parameter \mathcal{S} for which \mathcal{A} is minimum.

λ/M	$Q_e = Q_m = 0$		$Q_e = 0.4$ and $Q_m = 0$		$Q_e = 0.5$ and $Q_m = 0$		$Q_e = 0.6$ and $Q_m = 0$	
	r_{min}/M	$\mathcal{S}(\pm)$	r_{min}/M	$\mathcal{S}(\pm)$	r_{min}/M	$\mathcal{S}(\pm)$	r_{min}/M	$\mathcal{S}(\pm)$
0.0000001	3.00000	± 5.19615	2.88924	± 5.05297	2.82287	± 4.96791	2.73693	± 4.85869
0.000001	2.99998	± 5.19611	2.88922	± 5.05294	2.82285	± 4.96787	2.73691	± 4.85865
0.00001	2.99982	± 5.19582	2.88905	± 5.05264	2.82268	± 4.96757	2.73673	± 4.85834
0.0001	2.99850	± 5.19347	2.88769	± 5.05023	2.82129	± 4.96512	2.73529	± 4.85584
0.001	2.98850	± 5.17536	2.87734	± 5.03167	2.81069	± 4.94627	2.72435	± 4.83656
0.01	2.91985	± 5.04869	2.80642	± 4.90209	2.73821	± 4.81474	2.64956	± 4.70223
0.1	2.56341	± 4.35581	2.43967	± 4.19613	2.36405	± 4.09965	2.26402	± 3.97353
0.2	2.35962	± 3.92406	2.23287	± 3.76087	2.15482	± 3.66158	2.05061	± 3.53078
0.3	2.24441	± 3.65108	2.11924	± 3.49040	2.04208	± 3.39255	1.93891	± 3.26346
0.4	2.18206	± 3.47439	2.06104	± 3.31964	1.98667	± 3.22564	1.88760	± 3.10198
0.5	2.15448	± 3.36190	2.03889	± 3.21475	1.96825	± 3.12578	1.87473	± 3.00935
0.6	2.15094	± 3.29430	2.04128	± 3.15535	1.97468	± 3.07181	1.88716	± 2.96313
λ/M	$Q_e = 0.2$ and $Q_m = 0.5$		$Q_e = 0.4$ and $Q_m = 0.5$		$Q_e = 0.5$ and $Q_m = 0.5$		$Q_e = 0.6$ and $Q_m = 0.5$	
	r_{min}/M	$\mathcal{S}(\pm)$	r_{min}/M	$\mathcal{S}(\pm)$	r_{min}/M	$\mathcal{S}(\pm)$	r_{min}/M	$\mathcal{S}(\pm)$
0.0000001	2.79228	± 4.92891	2.69582	± 4.80686	2.61803	± 4.70959	2.51489	± 4.58250
0.000001	2.79226	± 4.92887	2.69580	± 4.80683	2.61801	± 4.70956	2.51486	± 4.58246
0.00001	2.79209	± 4.92857	2.69562	± 4.80651	2.61782	± 4.70924	2.51466	± 4.85213
0.0001	2.79068	± 4.92609	2.69416	± 4.80398	2.61631	± 4.70664	2.51307	± 4.57944
0.001	2.77997	± 4.90709	2.68303	± 4.78448	2.60479	± 4.68669	2.50095	± 4.55881
0.01	2.70670	± 4.77461	2.60701	± 4.64869	2.52616	± 4.54788	2.41816	± 4.41539
0.1	2.32875	± 4.05493	2.21513	± 3.91261	2.12024	± 3.79596	1.98782	± 3.63747
0.2	2.11818	± 3.61535	1.99918	± 3.46709	1.89807	± 3.34389	1.75277	± 3.17281
0.3	2.00583	± 3.34695	1.88791	± 3.20050	1.78739	± 3.07846	1.64207	± 2.90815
0.4	1.95181	± 3.18191	1.83881	± 3.04186	1.74314	± 2.92573	1.60636	± 2.76492
0.5	1.93526	± 3.08452	1.82898	± 2.95303	1.74001	± 2.84496	1.61522	± 2.69736
0.6	1.94372	± 3.03320	1.84466	± 2.91089	1.76277	± 2.81134	1.65015	± 2.67738

The first-look analysis of Eqn. (67) confirms that P^r is real, and therefore u^r if and only if the motion of the spinning particle is constrained in such a way that $\mathcal{E} > V_{eff(+)}$ or $\mathcal{E} < V_{eff(-)}$, as mentioned in previous section as well together with the condition with $\mathcal{A} > 0$, which is an extra condition coming solely because of the spin-orbit coupling. In Table II, we discover the values of the radial parameter (i.e. r_{min}) for various combinations of λ, Q_e and Q_m , as well as the corresponding range of spin parameter per unit mass \mathcal{S} for which the condition $\mathcal{A} > 0$ is fulfilled. For a consistency check, we demonstrated in Table II that when Q_e and Q_m vanish and the PFDM parameter is extremely tiny (i.e., $\lambda = 0.0000001$), the exact Schwarzschild limiting values (i.e., $r_{min} = 3$ and $-5.19615 < \mathcal{S} < 5.19615$) as found in [92] are recovered. Furthermore, in the limit $Q_m \rightarrow 0$ and $\lambda \rightarrow 0$, the V_{eff} obtained in Eqn. (68) reduces to that of the Reissner-Nordström black hole (BH). However, if $Q_e \rightarrow 0$ in addition to $Q_m \rightarrow 0$ and $\lambda \rightarrow 0$, $V_{eff(+)}$ matches that of the Schwarzschild BH [92]. The effective potential $V_{eff(+)}$ for both direct (i.e. $\mathcal{L} = \mathcal{J} - \mathcal{S} > 0$) as well as retrograde (i.e. $\mathcal{L} = \mathcal{J} - \mathcal{S} < 0$) trajectories of a spinning particle is plotted in Figs. 7–9, for various com-

binations of Q_e, Q_m, λ and \mathcal{S} . A brief summary of the results obtained after analyzing the plots in Figs. 7–9 of $V_{eff(+)}$ are as follows:

- (i) In Fig. 7, for the direct trajectories, we observe that when the parameter \mathcal{S} grows, the maximum of $V_{eff(+)}$ first drops and then climbs again, as well as moves closer to the BH's event horizon r_h (see left panel). In contrast, the maximum of $V_{eff(+)}$ goes away from the r_h as the parameter \mathcal{S} increases for retrograde trajectories (see right panel).
- (ii) In Fig. 8, we fix the parameters Q_e, Q_m and \mathcal{S} while varying the PFDM parameter λ . The maximum of $V_{eff(+)}$ grows as the parameter λ increases for the direct orbits, as shown in the left panel. The variation of r_h for the corresponding values of λ is shown in the inset plot; we find that increasing the parameter λ decreases the size of the event horizon r_h . A similar behavior is observed for the retrograde case of the $V_{eff(+)}$ in the right panel when the parameter λ increases; the only difference is that the maximum of $V_{eff(+)}$ is at higher values in comparison to the direct case for the equivalent

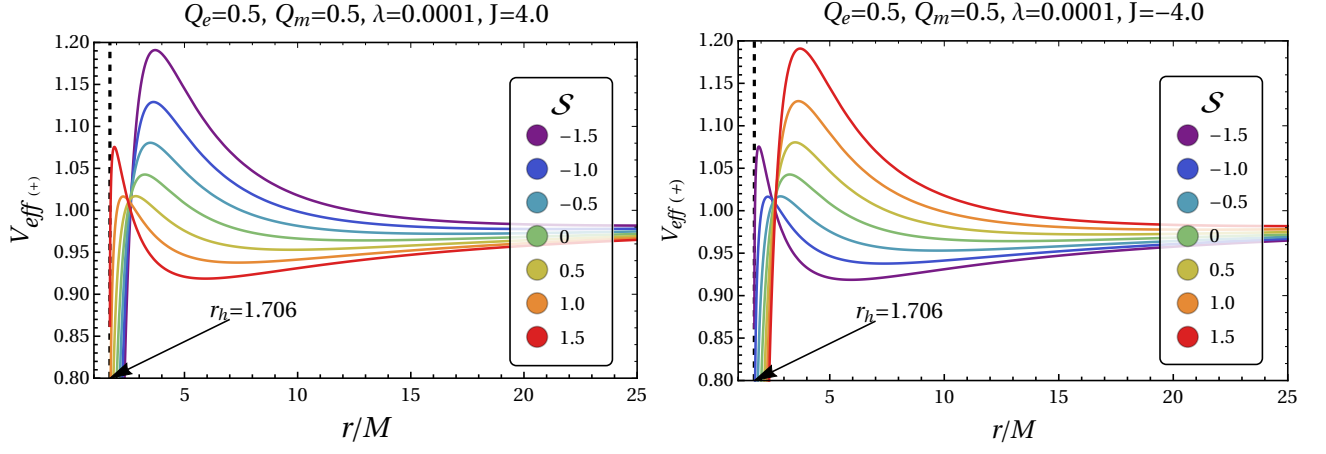


FIG. 7: Effective potential $V_{eff(+)}$ as a function of the spatial distance r/M . The left panel corresponds to direct trajectories, whereas the right panel refers to the retrograde trajectories for the different values of parameter \mathcal{S} , which varies from -1.5 to 1.5 in the steps of 0.5.

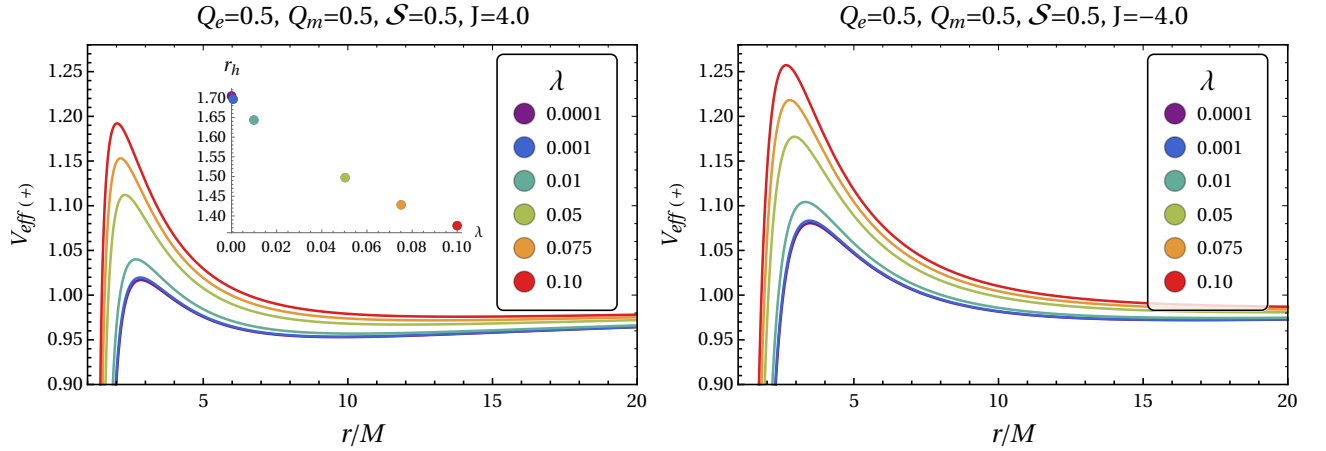


FIG. 8: Effective potential $V_{eff(+)}$ as a function of the spatial distance r/M . The left panel corresponds to direct trajectories, whereas the right panel is for retrograde trajectories. The inset graphic in the left panel depicts the evolution of the event horizon r_h as the PDFM parameter λ increases.

values of λ .

- (iii) Similarly, in Fig. 9, the behavior of $V_{eff(+)}$ for both direct (see left column) as well as retrograde trajectories (see right column) is plotted as a function of r/M is shown for various combinations of the parameters Q_m , λ and \mathcal{S} while varying the electric charge parameter Q_e . The maximum of $V_{eff(+)}$ is shown to grow when the parameter Q_e rises for both direct and retrograde trajectories. Additionally, it is seen from the inset plot in the top row, left panel that the event horizon r_h decreases with an increase in parameter Q_e . It is also seen that the maximum of $V_{eff(+)}$ occurs at a higher value for the retrograde trajectories when $\mathcal{S} > 0$ (see top row of Fig. 9), while for the case when $\mathcal{S} < 0$, it occurs for the direct trajectories (see bottom row of Fig. 9).

Now, by analyzing Eqn. (67) further, one finds that the divergence of $(P^r/m)^2$ when $\mathcal{B} = 0$ means that it gives the location r_{div} . As it is not easy to find the analytical value r_{div} , we thus numerically analyze it, and the results are presented in Figs. 10 and 11. In Fig. 10, we plot r_{div} as a function of the parameter \mathcal{S} for the fixed values of $Q_e = 0$ and 0.5, and $\lambda = 0.0001$ and vary the magnetic charge parameter Q_m . We find that r_{div} increases as the parameter $\pm\mathcal{S}$ increases. Similarly, in Fig. 11, we plot the r_{div} as a function of the parameter \mathcal{S} but here we choose different combinations of Q_e and Q_m , and vary the λ . A similar behavior r_{div} is observed with the parameter $\pm\mathcal{S}$ as in Fig. 10. It is vital to notice that the parameters Q_e and Q_m were chosen in such a way that a black hole horizon should exist. However, the PFDM parameter λ is selected in such a way that it must satisfy the requirement $\lambda \ll M$, as stated in Sec. II. Whereas the parameter \mathcal{S} is selected in such a manner that it must be

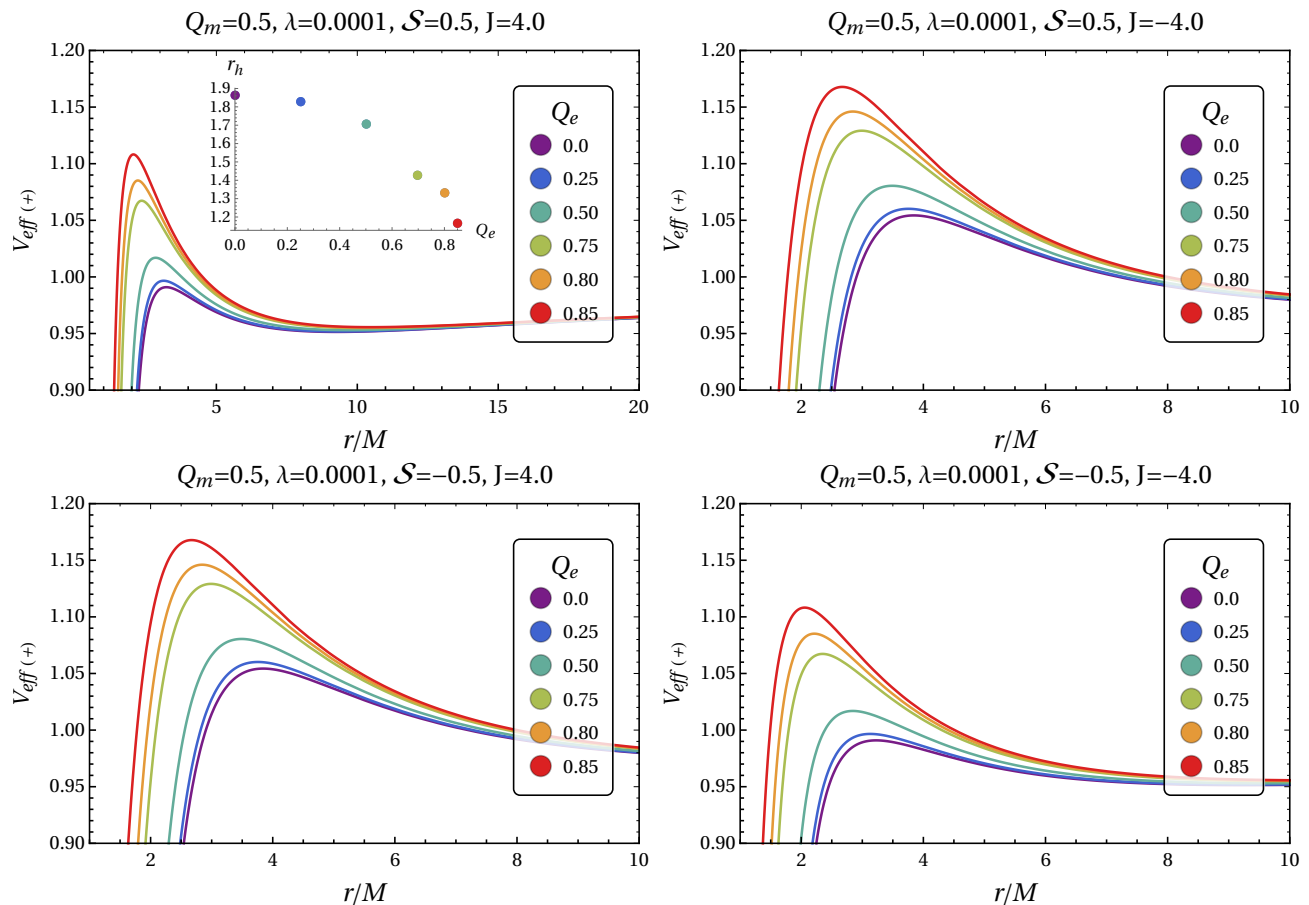


FIG. 9: Effective potential $V_{eff(+)}$ as a function of the spatial distance r/M . The left column corresponds to direct trajectories, whereas the right column is for retrograde trajectories. The inset graphic in the left panel of the top row depicts the evolution of the event horizon r_h as the parameter Q_e increases. Here, in the top row the spin per unit mass S is fixed to value 0.5, and in the bottom row the spin per unit mass S is fixed to value -0.5 , respectively.

smaller than M (known as the Møller limit [95, 96]), for the cases like the intermediate mass ratio inspirals, there is no such constraint on the choices of parameter S . As a result, we picked both scenarios where the parameter $S < M$ and $S > M$.

B. ISCO of a spinning particle moving in the background of a charged dyonic black hole immersed in PFDM

In this subsection, our primary interest is to study the behavior of the parameters r_{ISCO} , L_{ISCO} , E_{ISCO} , and Ω_{ISCO} of a spinning particle numerically, and also, due to the complexity of the equations of motion, it is more convenient to define the effective potential similar to [53]. Hence, we redefine the effective potential using Eqn. (60) as

$$W_{eff} \equiv \left(\frac{Pr}{m} \right)^2. \quad (74)$$

Now, in order to find the ISCOs of the spinning par-

ticle, the analogy of Eqns. (28) and (29) implies that we need to solve the following two equations simultaneously:

$$\frac{dr}{d\tau} = 0 \implies W_{eff} = 0 \quad (75)$$

$$\text{and } \frac{d^2r}{d\tau^2} = 0 \implies \frac{dW_{eff}}{dr} = 0, \quad (76)$$

together with the condition [coming from the analogy of Eqn. (34)]

$$\frac{d^2W_{eff}}{dr^2} = 0, \quad (77)$$

which gives the location of a flex point at which the maximum and minimum of W_{eff} coincide. Thus, Eqns. (75)–(77) form a system of equations for determining the ISCO parameters r_{ISCO} , L_{ISCO} , and E_{ISCO} . The explicit forms Eqns. (75)–(77) are shown in appendix B as Eqns. (B1)–(B3). The evolution of r_{ISCO} , L_{ISCO} , and E_{ISCO} , which are thus dependent on the black hole parameters Q_e , Q_m , M , PFDM parameter λ , and the particle's spin S , is thus analyzed in

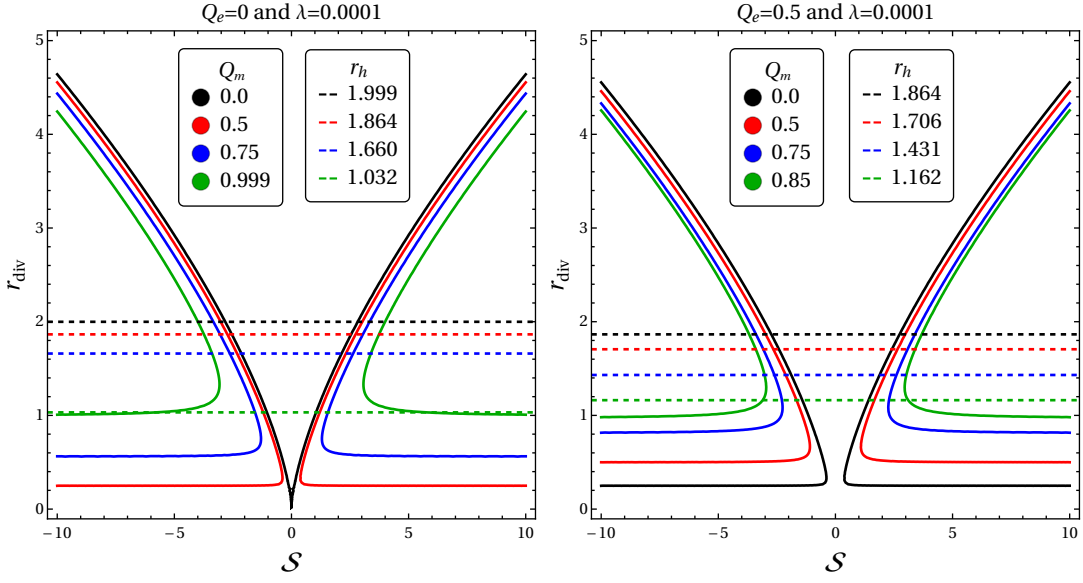


FIG. 10: Divergence radius r_{div} as a function of spin parameter S . In both panels left and right, we fix the parameter λ and vary parameter Q_m . However, the parameter $Q_e = 0$ and 0.5 for the left panel and the right panel, respectively. Here, the horizontal dashed lines represent the location of event horizon r_h for the corresponding combination of Q_e, Q_m and λ . The mass parameter M of a charged dyonic black hole immersed in PFDM is set to unity.

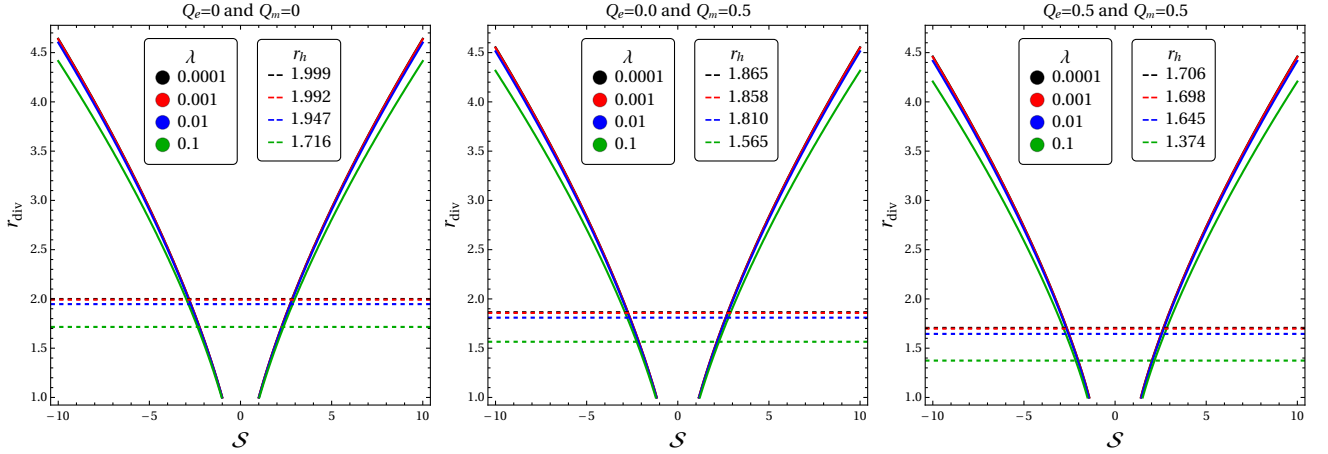


FIG. 11: Divergence radius r_{div} as a function of spin S for different combinations of $Q_e + Q_m$ and various parameters λ . The sum $Q_e + Q_m$ increases moving from left to right along the row. Here, also the mass parameter M of a charged dyonic black hole immersed in PFDM is set to unity.

Fig. 12 using these three equations, which constitute a closed system. It is worth mentioning here that for the spinning particle we use the total angular momentum J which is the sum of orbital momentum L and spin S (i.e. $J = L + S$) [97][103]

In addition, for r_{ISCO}, L_{ISCO} and E_{ISCO} there is one more important quantity related to the circular motion of the particle that is its orbital angular velocity Ω , also known as orbital angular frequency or Keplerian angular frequency. This Keplerian frequency Ω is identified via the relation

$$\Omega \equiv \dot{\phi}. \quad (78)$$

To find the Ω_{ISCO} for a spinning particle, we use the analogy of a geodesic particle, and hence substitute the values of r_{ISCO}, L_{ISCO} , and E_{ISCO} in Eqn. (78) found via Eqns. (75)–(77). We analyze the behavior of Ω as a function of S at the ISCO, as seen by an observer at infinity in Fig. 12 together with other ISCO parameters. Further, while studying the motion of a spinning particle in a curved spacetime it is important to take into consideration superluminal constraint. As we know from the literature [44, 53], for a spinning particle moving in curved spacetime, its four-momentum P^μ and four-velocity u^μ are no longer parallel to each other. Hence, four-velocity can be timelike (i.e., $u_\mu u^\mu < 0$) as well as spacelike (i.e.,

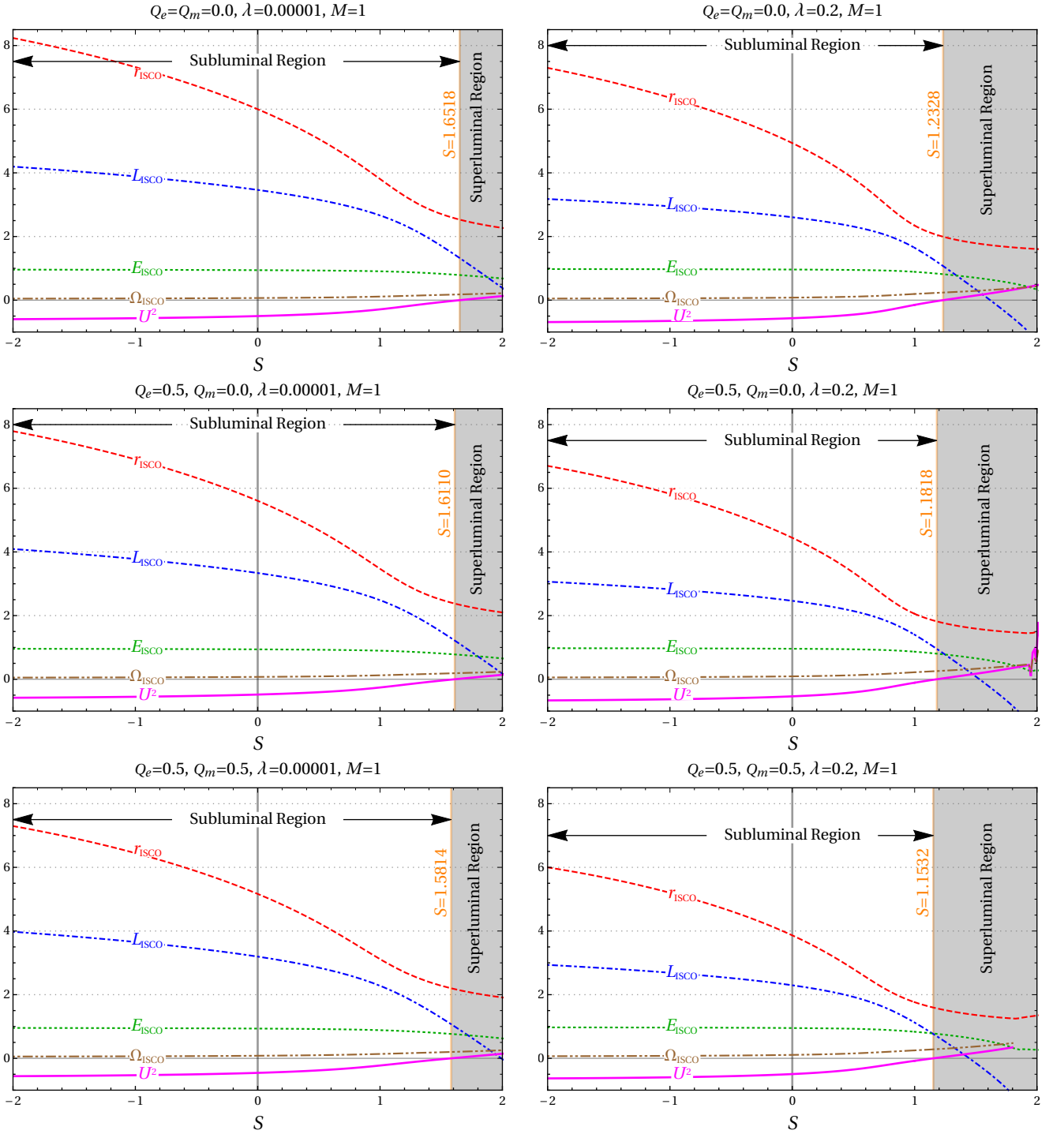


FIG. 12: Behavior of ISCO parameters r_{ISCO} , L_{ISCO} , E_{ISCO} and Ω_{ISCO} as well as four-velocity square U^2 as a function of the spin per unit mass S for the various combinations of Q_e , Q_m and λ . The PFDM parameter λ grows as we move from left to right along each row. However, as we move down along each of the columns, the sum $Q_e + Q_m$ increases. The black hole mass parameter M is fixed to unity.

$u_\mu u^\mu > 0$). The timelike (physical) four-velocity of a spinning particle is known as the subluminal, whereas the spacelike (unphysical) four-velocity of a spinning particle is known as superluminal. Therefore, to ensure that the

motion of the spinning particle is subluminal (physical), we impose a constraint

$$U^2 = \frac{u_\mu u^\mu}{(u^t)^2} = -F(r) + \frac{1}{F(r)} (\dot{r})^2 + r^2 (\dot{\phi})^2 < 0 \quad (79)$$

known as the superluminal constraint. The explicit form of the U^2 is given in appendix B as Eqn. (B4). The behavior of U^2 as a function of parameter \mathcal{S} in addition to the behavior of parameters r_{ISCO} , L_{ISCO} , E_{ISCO} , and Ω_{ISCO} is shown in Fig. 12, for various values of black hole parameters λ , Q_e and Q_m .

V. SUMMARY AND CONCLUSIONS

In this paper, we have investigated the motion of two different classes of test particles: (i) a massive test particle with charge, and (ii) a massive particle with spin S , moving in the space-time of a charged dyonic black hole immersed in PFDM. To investigate the aforementioned, we first described the line element of the black hole using Eqns. (10) and (11), and obtained the explicit expression for horizons (i.e. the Cauchy horizon r_- and the event horizon $r_+ = r_h$) in the limit $\lambda \ll M$. The bounds on the charge parameters Q_e and Q_m , and PFDM parameter λ for which a black hole exists is also obtained (see the shaded region in Fig. 1). It is observed that the horizon of the black hole is very sensitive to PFDM parameter λ as the shaded region for which black hole exists (i.e the event horizon r_h), first shrinks and then grows again as parameter λ rises (see Figs. 1 and 2).

We followed the Hamiltonian approach to study the dynamics of a charged moving around a charged dyonic black hole immersed in PFDM. To begin with, we first numerically analysed behaviour of $V_{eff}(r)$ for various combinations of black hole parameters $Q_{e,m}$ and λ in addition to the charge coupling parameters σ_e and g_m . It is observed from the top right and bottom panel of Fig. 3 that the maximum of the $V_{eff}(r)$ increases as well shifts towards the event horizon r_h as an effect of parameters $Q_{e,m}$ and λ . Contrary to this, when parameters $Q_{e,m}$ and λ are fixed and the coupling parameters σ_e and g_m vary the the maximum of $V_{eff}(r)$ reduces and shifts away from r_h (see top left panel of Fig. 3). We also plotted the trajectories of charge particle in Fig. 4, it found that a charged particle have three different kind of orbits: bound, captured and escaping orbits, namely. On the other hand, a captured orbit occurs when the magnitude of magnetic charge q_m increases, while a escaping orbit is observed for larger value of electric charge q . It is further observed that these orbits becomes bounded as consequence of increase PFDM parameter λ . From Fig. 5, it is found that circular orbits of charge particles shift toward larger radii for as the parameter g_m and q_e increase. However, an opposite behavior is observed when PFDM parameter λ increase. Finally, we presented the values ISCO parameters for the case of charged particles in Table I, it is found that radius of ISCO r_{ISCO} decreases with the rise in PFDM parameter λ while it increases with the increase in the charge coupling parameter g_m and σ_e . Whereas, the orbital angular momentum at ISCO \mathcal{L}_{ISCO} decreases with the increase in parameter λ keeping charge parameters $Q_{e,m}$ and coupling param-

eters σ_e and g_m of black hole fixed, an opposite behaviour is observed for \mathcal{E}_{ISCO} . Contrary to this, it is seen that the parameters \mathcal{L}_{ISCO} and \mathcal{E}_{ISCO} behave oppositely when increase the parameter σ_e and g_m keeping the black hole parameters $Q_{e,m}$ and λ fixed. Additionally, it is found that the orbital velocity v at ISCO always decreases as one move away as the value of the both the charge parameters $Q_{e,m}$ and PFDM λ increases (see Fig. 6).

To study the motion of massive spinning particle in the equatorial plane of the charged dyonic black hole immersed PFDM, we used the Lagrangian approach over the MP approach for the reasons stated in the appendix A. We explicitly obtained the expressions for the non-zero components of four-momentum P^μ and coordinated velocity v^μ . For various combinations of parameters $Q_{e,m}$, λ , and \mathcal{S} , we numerically analysed the nature of effective Potential $V_{eff(+)}$ in detail (see Figs. 7–9) for both direct (i.e. $\mathcal{L} = \mathcal{J} - \mathcal{S} > 0$) and retrograde (i.e $\mathcal{L} = \mathcal{J} - \mathcal{S} < 0$) trajectories. When comparing Figs. 7 and 8, it was discovered that $V_{eff(+)}$ is extremely sensitive to particle spin and the PFDM parameter λ , and showed different behaviour when one parameter is fixed while the other is varied.

Further, as Mathisson and Papapetrou Eqns. (A4) and (A5) lead to superluminal motion (i.e. space like behaviour) of the spinning particle as they neglect the “multi-pole” moments and consider only the “spin-dipole” moment. In Sec. IV B, we analysed the ISCOs parameters r_{ISCO} , L_{ISCO} , E_{ISCO} and Ω_{ISCO} of spinning particle in detail to find the region where spinning particle motion is timelike and bring out the effect of PFDM λ together with black hole charge parameters $Q_{e,m}$ on ISCOs. It is seen that the parameters r_{ISCO} and L_{ISCO} become smaller as the PFDM parameter λ increases for the corresponding value of particle spin parameter S and black hole charge parameters $Q_{e,m}$, which is consistent with the already established fact in [27, 36] that it can lead to an attractive force. Whereas, the parameters E_{ISCO} and L_{ISCO} increase (compare left column versus right column in Fig. 12). Analyzing more, the left column versus the right column of Fig. 12, it is interestingly observed that when the dark matter parameter λ grows, the spinning particle enters the superluminal region (i.e. $U^2 > 0$, spacelike) for smaller values of spin, contrary to the fact established in the previous works that the superluminal region is reached for larger values of spin \mathcal{S} if the dark matter field is absent [60]. While when one moved down the columns in Fig. 12, the values of r_{ISCO} , L_{ISCO} , E_{ISCO} and Ω_{ISCO} decrease with increase in the sum $(Q_e + Q_m)$ of black hole charges. However, the limiting value of particle spin for which the motion is subluminal decreases slightly, contrary to what is observed when one moves along the row by varying the PFDM parameter λ keeping $Q_{e,m}$ fixed.

Finally, it is concluded that when the PFDM parameter λ is very tiny (say 0.00001) and the black hole charges disappear $Q_e = Q_m = 0$, the ISCO parameters r , L , E , and Ω displayed in the top left panel of Fig. 12 matched

the Schwarzschild black hole scenario (Fig. 2 of [60]), implying that for very small value of PFDM parameter λ the charged dyonic black hole immersed in PFDM is identical to Schwarzschild black hole. It is also worth noting that our findings of a charged dyonic black hole immersed in PFDM reproduced the exact same conclusion as Jefremov *et al.* [53] in the Schwarzschild limit. On the other hand, in the case $Q_m = 0$ and $\lambda = 0.00001$, our results (see the middle panel on the left column of Fig. 12) coincided with Zhang *et al.* [57] for Reissner-Nördstrom black hole. These observations on the PFDM parameter λ imply that for tiny enough values of λ (say, $\lambda \leq 0.00001$), the charged dyonic black hole immersed in PFDM acts identically to its counterparts without PFDM. However, for large enough λ values (say, $\lambda \geq 0.1$), the ISCO parameters r_{ISCO} and L_{ISCO} fall dramatically (as seen by comparing the left and right columns of Fig. 12), showing that small ISCOs are conceivable for large λ values.

Thus, the work done here for the charged particles and spinning particles moving around the charged dyonic black hole submerged in PFDM is novel and intriguing since the PFDM effect on the spinning particle has not yet been documented in the literature. Also, in the near future it will become possible to detect and accurately measure gravitational waves emitted from extreme-mass ratio inspirals as well as from intermediate-mass-ratio inspirals with the help of advanced space-based gravitational wave detectors like TianQin, Taiji, and LISA (Laser Interferometer Space Antenna). As a consequence, with the advancement of technology, we will be able to acquire information about the ISCOs and our results, including the PFDM. As a result, the work done here on ISCOs will be important in better understanding the nature and initial condition of binary black hole mergers and their surrounding.

Acknowledgments

We are grateful to the referee for his insightful remarks and constructive suggestions that helped us to improve the clarity and precision of this paper. S.S. acknowledges the support from Research Grant No. F-FA-2021-432 of the Uzbekistan Ministry for Innovative Development. P.S. acknowledges support under Council of Scientific and Industrial Research-RA scheme (Government of India).

Appendix A: A brief summary of Lagrangian theory of spinning particles in curved spacetime

The dynamics of a spinning particle in curved spacetime was first studied by Mathisson [84] and Papapetrou [85] (hereinafter referred to as MP). Later, it was further extended by Tulczyjew [98], Taub [99], and Dixon [100]. In the MP framework, the spinning test particle moving in curved spacetime follows a nongeodesic trajectory due

to the spin-orbit coupling. In their approach, the spinning particle is considered the particle of finite length that is much smaller than the characteristic length scale of spacetime; therefore, it is assumed that the spinning particle possesses a dipole moment in addition to the monopole moment that one needs to define the point particle.

In this appendix, for the sake of completeness (i.e., to make the paper self-contained), we present a brief summary of the Lagrangian theory of a spinning particle in curved spacetime. For a detailed study of the theory of a spinning particle in curved spacetime, we encourage the reader to go through the articles [79, 86–88]. In this work, we follow the Lagrangian approach to find the equations of motion for the spinning particles moving in the vicinity of a static spherically symmetric charged dyonic black hole immersed in PFDM. There are four main reasons for using the Lagrangian approach to find the equations of motion over the MP approach:

- (i) Rather than adopting an *ad hoc* or *a posteriori* definition, this approach allows for a precise description of the four-momentum. This is very useful, as the four-momentum and four-velocity are not parallel for the spinning particles moving in curved spacetime.
- (ii) The equations of motion are reparametrization covariant by nature.
- (iii) This theory gives a natural interpretation of angular velocity, which helps us interpret the spin of a particle as a three-dimensional rotation.
- (iv) In this theory, the Casimir operators of the Poincaré group generated with the canonical momenta are constants of motion, allowing an easy description of the particle's mass m and spin S .

In this theory a Lagrangian \mathcal{L} is constructed from four arbitrary invariant functions $\mathcal{C}_1 \equiv u_\mu u^\mu$, $\mathcal{C}_2 \equiv \sigma_{\mu\nu} \sigma^{\mu\nu} = -\text{tr}(\sigma^2)$, $\mathcal{C}_3 \equiv u_\alpha \sigma^{\alpha\beta} \sigma_{\beta\nu} u^\nu$, and $\mathcal{C}_4 \equiv \det(\sigma)$,

$$\mathcal{L} \equiv \mathcal{L}(\mathcal{C}_1, \mathcal{C}_2, \mathcal{C}_3, \mathcal{C}_4) = \sqrt{\mathcal{C}_1} L \left(\frac{\mathcal{C}_2}{\mathcal{C}_1}, \frac{\mathcal{C}_3}{\mathcal{C}_1^2}, \frac{\mathcal{C}_4}{\mathcal{C}_1^2} \right), \quad (\text{A1})$$

such that action $\mathcal{I} = \int \mathcal{L} d\tau$ is τ -reparametrization invariant. Here, u^μ is the four-velocity $u^\mu \equiv dx^\mu/d\tau$ of the spinning particle, $\sigma^{\mu\nu}$ is the antisymmetric angular velocity tensor, τ is an affine parameter for the spinning particle position four-vector $x^\mu = x^\mu(\tau)$ and L is an arbitrary function. It is worth noting here that, unlike the nonspinning particle case, it is not necessary for the spinning particle case to have a negative normalized four-velocity \mathcal{C}_1 in order to have a real \mathcal{L} [88].

The four-momentum P_μ and antisymmetric spin tensor $S_{\mu\nu}$ are defined via relations

$$P_\mu \equiv \frac{\partial \mathcal{L}}{\partial u^\mu}, \quad (\text{A2})$$

$$\text{and } S_{\mu\nu} \equiv \frac{\partial \mathcal{L}}{\partial \sigma^{\mu\nu}} = -S_{\nu\mu}. \quad (\text{A3})$$

As usual, by varying the action \mathcal{I} , the nongeodesic equations of motion for a spinning particle moving in curved spacetime are obtained [86, 87]

$$\frac{DP^\mu}{D\tau} = -\frac{1}{2}R^\mu_{\nu\alpha\beta}u^\nu S^{\alpha\beta}, \quad (\text{A4})$$

$$\frac{DS^{\mu\nu}}{D\tau} = S^{\mu\alpha}\sigma'_\alpha{}^\nu - \sigma^{\mu\alpha}S'_\alpha{}^\nu = P^\mu u^\nu - u^\mu P^\nu, \quad (\text{A5})$$

where, $D/D\tau \equiv u^\mu \nabla_\mu$ and $R^\mu_{\nu\alpha\beta}$ are the covariant derivatives along u^μ and the Riemann tensor, respectively. Interestingly, these results hold for the arbitrary function L as well and it is found that the dynamical variable four-momentum P^μ and spin tensor $S^{\mu\nu}$ are the generators of the Poincaré group.

It is also shown in [88] that for a spinning particle moving in curved spacetime both its mass m and spin S are two conserved quantities defined as

$$m^2 \equiv -P_\mu P^\mu, \quad (\text{A6})$$

$$S^2 \equiv \frac{1}{2}S_{\mu\nu}S^{\mu\nu}. \quad (\text{A7})$$

One can see here that conservation of S^2 is coming solely from the Eqn. (A5) equation of motion by contracting Eqn. (A5) with the covariant component of spin tensor $S_{\mu\nu}$. It is worth to emphasizing here that conservation of particle spin comes naturally in the Lagrangian theory [86], in contrast with the extended MP formulation [100], which requires an extra assumption.

Furthermore, simply glancing at Eqns. (A4) and (A5) reveals that there are more unknown variables than there are equations. Toover come this difficulty, the TSSC [98]

$$P_\mu S^{\mu\nu} = 0 \quad (\text{A8})$$

is used. The above Eqn. (A8) helps us set three of the six independent components of spin tensor to zero (i.e. $S^{0i} = 0$) for a particular frame of reference. Hence, it gives the freedom to fix the worldline describing the path of a spinning particle. The components of S^{0i} are associated with the mass dipole moment of the spinning particle, so setting these equal to zero in some particular frame of reference fixes the center of mass of the spinning particle in that frame of reference (for a detailed discussion on SSC, we request reader to see [101] and the references therein). Also, it is shown in [102] that Eqn. (A8) defines a unique worldline of the spinning particle in a curved spacetime. In addition to the four reasons stated earlier for using the Lagrangian theory to find equations of

motion, it worth noting here that if function L is chosen wisely, one would derive the TSSC from the Lagrangian [88], which is another motivation to use the Lagrangian theory approach. Now, one can define a normalized four-momentum as

$$V^\mu = \frac{P^\mu}{m}, \quad (\text{A9})$$

such that it satisfies the conservation relation ($V_\mu V^\mu = -1$). As the four-velocity u^μ is not the conserved quantity for the case of spinning particle. Hence, one need to bridle the u^μ as

$$u_\mu u^\mu < 0, \quad (\text{A10})$$

in addition to SSC Eqn. (A8) so that the spinning particle will have a timelike motion. For convince, one may choose

$$u_\mu V^\mu = -1, \quad (\text{A11})$$

as pointed in [97]. Now, using Eqns. (A4)–(A11), a relation between a u^μ and momentum V^μ can be establish which reads as

$$u^\mu - V^\mu = \frac{2S^{\mu\nu}R_{\nu\alpha\beta\gamma}V^\alpha S^{\beta\gamma}}{4m^2 + R_{\delta\rho\sigma\kappa}S^{\delta\rho}S^{\sigma\kappa}}. \quad (\text{A12})$$

Additionally, more conserved quantities can be found depending on the geometry of the spacetime by using

$$\mathfrak{C}_\xi \equiv P^\mu \xi_\mu - \frac{S^{\mu\nu}\xi_{\mu;\nu}}{2}, \quad (\text{A13})$$

where, ξ_μ is a Killing vector that satisfies the relation

$$2\xi_{(\mu;\nu)} = 0. \quad (\text{A14})$$

In order to make this paper self-contained, we presented a brief overview of Lagrangian theory. The equations of motion of the spinning particle moving in the vicinity of a charged dyonic black hole immersed in PFDM are determined using Eqns. (A2)–(A13).

Appendix B: Explicit expressions of ISCO equations and superluminal constraint

Here, we present the explicit form of ISCO Eqns. (75)–(77) as a function of the radial coordinate r , spin per unit mass \mathcal{S} , total angular per unit mass \mathcal{J} , energy per unit mass \mathcal{E} , and black hole parameters M, Q_e and Q_m :

$$W_{eff} = \frac{1}{(2r^5 + r\mathcal{S}^2\mathcal{Y})^2} \left[(2\mathcal{E}r^5 + \mathcal{J}r\mathcal{S}\mathcal{Y})^2 + (4r^6(\mathcal{J} - \mathcal{E}\mathcal{S})^2 + (2r^4 + \mathcal{S}^2\mathcal{Y})^2) \mathcal{X} \right] = 0, \quad (\text{B1})$$

$$\begin{aligned} \frac{dW_{eff}}{dr} = & \frac{1}{(2r^5 + r\mathcal{S}^2\mathcal{Y})^3} \left[-8r^6 \mathcal{X}(\mathcal{J} - \mathcal{E}\mathcal{S})^2 \left(2r^4 - \mathcal{S}^2 \left(2\lambda r \ln \left(\frac{r}{|\lambda|} \right) - 4Mr + 6Q_{e+m}^2 - 3\lambda r \right) \right) \right. \\ & - 2r^2 \mathcal{S}^2 \eta \Psi^2 + 2\mathcal{J}r^2 \mathcal{S} \Psi \eta \left(\lambda r \mathcal{S}^2 \ln \left(\frac{r}{|\lambda|} \right) - r\mathcal{S}^2(\lambda + 2M) + 2\mathcal{S}^2 Q_{e+m}^2 + 2r^4 \right) \\ & \left. + \mathcal{Y} (2r^4 + \mathcal{S}^2\mathcal{Y}) (4r^6(\mathcal{J} - \mathcal{E}\mathcal{S})^2 + (2r^4 + \mathcal{S}^2\mathcal{Y})^2) \right] = 0, \quad (\text{B2}) \end{aligned}$$

$$\begin{aligned} \frac{d^2W_{eff}}{dr^2} = & -\frac{1}{(2r^5 + r\mathcal{S}^2\mathcal{Y})^4} \left[-8r^6 \mathcal{X}(\mathcal{J} - \mathcal{E}\mathcal{S})^2 \left(\lambda r \mathcal{S}^2 \ln \left(\frac{r}{|\lambda|} \right) \right) (-r\mathcal{S}^2(19\lambda + 24M) + 36\mathcal{S}^2 Q_{e+m}^2 - 36r^4) \right. \\ & + 6\lambda^2 r^2 \mathcal{S}^4 \ln^2 \left(\frac{r}{|\lambda|} \right) + 2 \left(r^2 \mathcal{S}^4 (8\lambda^2 + 12M^2 + 19\lambda M) - r\mathcal{S}^4 (31\lambda + 36M) Q_{e+m}^2 + r^5 \mathcal{S}^2 (29\lambda + 36M) \right. \\ & - 60r^4 \mathcal{S}^2 Q_{e+m}^2 + 30\mathcal{S}^4 (Q_{e+m}^2)^2 + 6r^8 \left. \right) + 16r^6 \mathcal{Y}(\mathcal{J} - \mathcal{E}\mathcal{S})^2 (2r^4 + \mathcal{S}^2\mathcal{Y}) \left(2r^4 - \mathcal{S}^2 \left(2\lambda r \ln \left(\frac{r}{|\lambda|} \right) \right. \right. \\ & - 4Mr + 6Q_{e+m}^2 - 3\lambda r \left. \right) \left. \right) + (2r^4 + \mathcal{S}^2\mathcal{Y})^2 (4r^6(\mathcal{J} - \mathcal{E}\mathcal{S})^2 + (2r^4 + \mathcal{S}^2\mathcal{Y})^2) \left(2\lambda r \ln \left(\frac{r}{|\lambda|} \right) - 4Mr \right. \\ & + 6Q_{e+m}^2 - 3\lambda r \left. \right) - 2\mathcal{J}\mathcal{S} (2r^5 + r\mathcal{S}^2\mathcal{Y})^2 \left(\left(12\lambda r \ln \left(\frac{r}{|\lambda|} \right) - 24Mr + 40Q_{e+m}^2 - 19\lambda r \right) \left(\mathcal{J}\lambda r \mathcal{S} \ln \left(\frac{r}{|\lambda|} \right) \right. \right. \\ & + 2\mathcal{E}r^4 + \mathcal{J}\mathcal{S} (-r(\lambda + 2M) + 2Q_{e+m}^2) \left. \right) + \mathcal{J}\mathcal{S} \left(3\lambda r \ln \left(\frac{r}{|\lambda|} \right) - 6Mr + 8Q_{e+m}^2 - 4\lambda r \right)^2 \left. \right) \\ & - 2(2\mathcal{E}r^5 + \mathcal{J}r\mathcal{S}\mathcal{Y})^2 \left(\mathcal{S}^2 \left(-12\lambda r \ln \left(\frac{r}{|\lambda|} \right) + 24Mr - 40Q_{e+m}^2 + 19\lambda r \right) \left(\lambda r \mathcal{S}^2 \ln \left(\frac{r}{|\lambda|} \right) - r\mathcal{S}^2(\lambda + 2M) \right. \right. \\ & + 2\mathcal{S}^2 Q_{e+m}^2 + 2r^4 \left. \right) + 3\mathcal{S}^4 \left(3\lambda r \log \left(\frac{r}{|\lambda|} \right) - 6Mr + 8Q_{e+m}^2 - 4\lambda r \right)^2 \left. \right) + 8\mathcal{J}r^2 \mathcal{S}^3 \left(3\lambda r \ln \left(\frac{r}{|\lambda|} \right) - 6Mr \right. \\ & + 8Q_{e+m}^2 - 4\lambda r \left. \right)^2 \left(\lambda r \mathcal{S}^2 \ln \left(\frac{r}{|\lambda|} \right) - r\mathcal{S}^2(\lambda + 2M) + 2\mathcal{S}^2 Q_{e+m}^2 + 2r^4 \right) \left(\mathcal{J}\lambda r \mathcal{S} \ln \left(\frac{r}{|\lambda|} \right) + 2\mathcal{E}r^4 \right. \\ & \left. \left. + \mathcal{J}\mathcal{S} (-r(\lambda + 2M) + 2Q_{e+m}^2) \right) \right] = 0, \quad (\text{B3}) \end{aligned}$$

and the explicit form of U^2 Eqn. (79) using Eqns. (11), (64) and (65) reads

$$\begin{aligned} U^2 = & -F(r) + \frac{4r^2 \mathcal{X}^2 (\mathcal{J} - \mathcal{E}\mathcal{S})^2 \left(-2\lambda r \mathcal{S}^2 \log \left(\frac{r}{|\lambda|} \right) + r\mathcal{S}^2 (3\lambda + 4M) - 6\mathcal{S}^2 Q_{e+m}^2 + 2r^4 \right)^2}{\left(\lambda r \mathcal{S}^2 \log \left(\frac{r}{|\lambda|} \right) - r\mathcal{S}^2 (\lambda + 2M) + 2\mathcal{S}^2 Q_{e+m}^2 + 2r^4 \right)^2 \Psi^2} \\ & - \left[\frac{\mathcal{X} \left((2\mathcal{E}r^5 + \mathcal{J}r\mathcal{S}\mathcal{Y})^2 + \mathcal{X} (4r^6(\mathcal{J} - \mathcal{E}\mathcal{S})^2 + (2r^4 + \mathcal{S}^2\mathcal{Y})^2) \right)}{r^2 (2r^5 + r\mathcal{S}^2\mathcal{Y})^2 \Psi^2} \right] \\ & \times \left(\lambda r \mathcal{S}^2 \ln \left(\frac{r}{|\lambda|} \right) - r\mathcal{S}^2 (\lambda + 2M) + 2\mathcal{S}^2 Q_{e+m}^2 + 2r^4 \right)^2, \quad (\text{B4}) \end{aligned}$$

where,

$$\eta = -3\lambda r \ln\left(\frac{r}{|\lambda|}\right) + 6Mr - 8Q_{e+m}^2 + 4\lambda r, \quad (\text{B5})$$

$$\Psi = \mathcal{J}\lambda r \mathcal{S} \ln\left(\frac{r}{|\lambda|}\right) + 2\mathcal{E}r^4 + \mathcal{J}\mathcal{S}(-r(\lambda + 2M) + 2Q_{e+m}^2). \quad (\text{B6})$$

-
- [1] B. P. Abbott and et al. (Virgo and LIGO Scientific Collaborations), *Phys. Rev. Lett.* **116**, 061102 (2016), [arXiv:1602.03837 \[gr-qc\]](#) .
- [2] B. P. Abbott and et al. (Virgo and LIGO Scientific Collaborations), *Phys. Rev. Lett.* **116**, 241102 (2016), [arXiv:1602.03840 \[gr-qc\]](#) .
- [3] K. Akiyama and et al. (Event Horizon Telescope Collaboration), *Astrophys. J.* **875**, L1 (2019), [arXiv:1906.11238 \[astro-ph.GA\]](#) .
- [4] K. Akiyama and et al. (Event Horizon Telescope Collaboration), *Astrophys. J.* **875**, L6 (2019), [arXiv:1906.11243 \[astro-ph.GA\]](#) .
- [5] C. A. Benavides-Gallego, A. Abdujabbarov, D. Malafarina, B. Ahmedov, and C. Bambi, *Phys. Rev. D* **99**, 044012 (2019), [arXiv:1812.04846 \[gr-qc\]](#) .
- [6] N. Tsukamoto and T. Harada, *Galaxies* **1**, 261 (2013), [arXiv:1201.1738 \[gr-qc\]](#) .
- [7] D. Bini, K. Boshkayev, and A. Geralico, *Class. Quantum Grav.* **29**, 145003 (2012), [arXiv:1306.4803 \[gr-qc\]](#) .
- [8] J. Kovář, Z. Stuchlík, and V. Karas, *Class. Quantum Grav.* **25**, 095011 (2008), [arXiv:0803.3155](#) .
- [9] S. Shaymatov, M. Patil, B. Ahmedov, and P. S. Joshi, *Phys. Rev. D* **91**, 064025 (2015), [arXiv:1409.3018 \[gr-qc\]](#) .
- [10] N. Dadhich, A. Tursunov, B. Ahmedov, and Z. Stuchlík, *Mon. Not. Roy. Astron. Soc.* **478**, L89 (2018), [arXiv:1804.09679 \[astro-ph.HE\]](#) .
- [11] P. Pavlović, A. Saveliev, and M. Sossich, *Phys. Rev. D* **100**, 084033 (2019), [arXiv:1908.01888 \[gr-qc\]](#) .
- [12] S. Shaymatov, *Int. J. Mod. Phys. Conf. Ser.* **49**, 1960020 (2019).
- [13] S. Shaymatov, J. Vrba, D. Malafarina, B. Ahmedov, and Z. Stuchlík, *Phys. Dark Universe* **30**, 100648 (2020), [arXiv:2005.12410 \[gr-qc\]](#) .
- [14] B. Turimov, B. Toshmatov, B. Ahmedov, and Z. Stuchlík, *Phys. Rev. D* **100**, 084038 (2019), [arXiv:1910.00939 \[gr-qc\]](#) .
- [15] J. Rayimbaev, M. Figueroa, Z. Stuchlík, and B. Juraev, *Phys. Rev. D* **101**, 104045 (2020).
- [16] V. C. Rubin, J. Ford, W. K., and N. Thonnard, *Astrophys. J.* **238**, 471 (1980).
- [17] M. Persic, P. Salucci, and F. Stel, *Mon. Not. R. Astron. Soc.* **281**, 27 (1996), [arXiv:astro-ph/9506004 \[astro-ph\]](#) .
- [18] V. V. Kiselev, *Class. Quantum Grav.* **20**, 1187 (2003), [gr-qc/0210040](#) .
- [19] M.-H. Li and K.-C. Yang, *Phys. Rev. D* **86**, 123015 (2012), [arXiv:1204.3178 \[astro-ph.CO\]](#) .
- [20] Z. Xu, X. Hou, and J. Wang, *Class. Quantum Grav.* **35**, 115003 (2018), [arXiv:1711.04538 \[gr-qc\]](#) .
- [21] S. Haroon, M. Jamil, K. Jusufi, K. Lin, and R. B. Mann, *Phys. Rev. D* **99**, 044015 (2019), [arXiv:1810.04103 \[gr-qc\]](#) .
- [22] R. A. Konoplya, *Phys. Lett. B* **795**, 1 (2019), [arXiv:1905.00064 \[gr-qc\]](#) .
- [23] S. H. Hendi, A. Nemati, K. Lin, and M. Jamil, *Eur. Phys. J. C* **80**, 296 (2020), [arXiv:2001.01591 \[gr-qc\]](#) .
- [24] K. Jusufi, M. Jamil, P. Salucci, T. Zhu, and S. Haroon, *Phys. Rev. D* **100**, 044012 (2019).
- [25] S. Shaymatov, B. Ahmedov, and M. Jamil, *Eur. Phys. J. C* **81**, 588 (2021).
- [26] J. Rayimbaev, S. Shaymatov, and M. Jamil, *Eur. Phys. J. C* **81**, 699 (2021), [arXiv:2107.13436 \[gr-qc\]](#) .
- [27] S. Shaymatov, D. Malafarina, and B. Ahmedov, *Phys. Dark Universe* **34**, 100891 (2021), [arXiv:2004.06811 \[gr-qc\]](#) .
- [28] D. Pugliese, H. Quevedo, and R. Ruffini, *Phys. Rev. D* **83**, 104052 (2011), [arXiv:1103.1807 \[gr-qc\]](#) .
- [29] D. Pugliese, H. Quevedo, and R. Ruffini, *Phys. Rev. D* **83**, 024021 (2011), [arXiv:1012.5411 \[astro-ph.HE\]](#) .
- [30] M. Zajacek and A. Tursunov, *The Observatory* **139**, 231 (2019), [arXiv:1904.04654 \[astro-ph.GA\]](#) .
- [31] J. Bally and E. R. Harrison, *Astrophys. J.* **220**, 743 (1978).
- [32] J. C. Weingartner, B. T. Draine, and D. K. Barr, *Astrophys. J.* **645**, 1188 (2006), [arXiv:astro-ph/0601296 \[astro-ph\]](#) .
- [33] R. M. Wald, *Phys. Rev. D* **10**, 1680 (1974).
- [34] M. Zajaček, A. Tursunov, A. Eckart, and S. Britzen, *Mon. Not. R. Astron. Soc.* **480**, 4408 (2018), [arXiv:1808.07327 \[astro-ph.GA\]](#) .
- [35] M. Kasuya, *Phys. Rev. D* **25**, 995 (1982).
- [36] B. Narzilloev, J. Rayimbaev, S. Shaymatov, A. Abdujabbarov, B. Ahmedov, and C. Bambi, *Phys. Rev. D* **102**, 044013 (2020), [arXiv:2007.12462 \[gr-qc\]](#) .
- [37] B. Narzilloev, J. Rayimbaev, S. Shaymatov, A. Abdujabbarov, B. Ahmedov, and C. Bambi, *Phys. Rev. D* **102**, 104062 (2020), [arXiv:2011.06148 \[gr-qc\]](#) .
- [38] V. P. Frolov and A. A. Shoom, *Phys. Rev. D* **82**, 084034 (2010), [arXiv:1008.2985 \[gr-qc\]](#) .
- [39] A. N. Aliev and N. Özdemir, *Mon. Not. R. Astron. Soc.* **336**, 241 (2002), [gr-qc/0208025](#) .
- [40] S. Shaymatov, F. Atamurotov, and B. Ahmedov, *Astrophys Space Sci* **350**, 413 (2014).
- [41] K. Düztaş, M. Jamil, S. Shaymatov, and B. Ahmedov, *Class. Quantum Grav.* **37**, 175005 (2020), [arXiv:1808.04711 \[gr-qc\]](#) .
- [42] S. Shaymatov, N. Dadhich, B. Ahmedov, and M. Jamil, *Eur. Phys. J. C* **80**, 481 (2020), [arXiv:1908.01195 \[gr-qc\]](#) .

- [43] S. Shaymatov and F. Atamurotov, *Galaxies* **9**, 40 (2021), [arXiv:2007.10793 \[gr-qc\]](#) .
- [44] S. Suzuki and K.-i. Maeda, *Phys. Rev. D* **58**, 023005 (1998), [arXiv:gr-qc/9712095](#) .
- [45] M. Campanelli, C. O. Lousto, and Y. Zlochower, *Phys. Rev. D* **73**, 061501(R) (2006), [gr-qc/0601091](#) .
- [46] C. Cabanac, R. P. Fender, R. J. H. Dunn, and E. G. Kording, *Mon. Not. Roy. Astron. Soc.* **396**, 1415 (2009), [arXiv:0904.0701 \[astro-ph.HE\]](#) .
- [47] S. Akcay, L. Barack, T. Damour, and N. Sago, *Phys. Rev. D* **86**, 104041 (2012), [arXiv:1209.0964 \[gr-qc\]](#) .
- [48] C. Chakraborty, *Eur. Phys. J. C* **74**, 2759 (2014), [arXiv:1307.4698 \[gr-qc\]](#) .
- [49] O. B. Zaslavskii, *Eur. Phys. J. C* **75**, 403 (2015), [arXiv:1405.2543 \[gr-qc\]](#) .
- [50] T. Delsate, J. V. Rocha, and R. Santarelli, *Phys. Rev. D* **92**, 084028 (2015), [arXiv:1507.03602 \[gr-qc\]](#) .
- [51] S. Shaymatov, B. Narzilloev, A. Abdujabbarov, and C. Bambi, *Phys. Rev. D* **103**, 124066 (2021), [arXiv:2105.00342 \[gr-qc\]](#) .
- [52] N. Dadhich and S. Shaymatov, *Phys. Dark Universe* **35**, 100986 (2022), [arXiv:2104.00427 \[gr-qc\]](#) .
- [53] P. I. Jefremov, O. Y. Tsupko, and G. S. Bisnovatyi-Kogan, *Phys. Rev. D* **91**, 124030 (2015), [arXiv:1503.07060 \[gr-qc\]](#) .
- [54] G. d'Ambrosi, S. Satish Kumar, J. van de Vis, and J. W. van Holten, *Phys. Rev. D* **93**, 044051 (2016), [arXiv:1511.05454 \[gr-qc\]](#) .
- [55] E. Harms, G. Lukes-Gerakopoulos, S. Bernuzzi, and A. Nagar, *Phys. Rev. D* **94**, 104010 (2016), [arXiv:1609.00356 \[gr-qc\]](#) .
- [56] G. Lukes-Gerakopoulos, E. Harms, S. Bernuzzi, and A. Nagar, *Phys. Rev. D* **96**, 064051 (2017), [arXiv:1707.07537 \[gr-qc\]](#) .
- [57] Y.-P. Zhang, S.-W. Wei, W.-D. Guo, T.-T. Sui, and Y.-X. Liu, *Phys. Rev. D* **97**, 084056 (2018), [arXiv:1711.09361 \[gr-qc\]](#) .
- [58] B. Toshmatov and D. Malafarina, *Phys. Rev. D* **100**, 104052 (2019), [arXiv:1910.11565 \[gr-qc\]](#) .
- [59] U. Nucamendi, R. Becerril, and P. Sheoran, *Eur. Phys. J. C* **80**, 35 (2020), [arXiv:1910.00156 \[gr-qc\]](#) .
- [60] C. Conde, C. Galvis, and E. Larrañaga, *Phys. Rev. D* **99**, 104059 (2019), [arXiv:1905.01323 \[gr-qc\]](#) .
- [61] E. Larrañaga, *Int. J. Mod. Phys. D* **29**, 2050121 (2020).
- [62] Y.-P. Zhang, S.-W. Wei, and Y.-X. Liu, *Universe* **6**, 103 (2020), [arXiv:2003.10960 \[gr-qc\]](#) .
- [63] M. Zhang and J. Jiang, *Phys. Rev. D* **101**, 104012 (2020), [arXiv:2004.13016 \[gr-qc\]](#) .
- [64] S. Suzuki and K.-i. Maeda, *Phys. Rev. D* **61**, 024005 (2000), [arXiv:gr-qc/9910064](#) .
- [65] D. Singh, *Phys. Rev. D* **72**, 084033 (2005), [arXiv:gr-qc/0509046](#) .
- [66] H. Koyama, K. Kiuchi, and T. Konishi, *Phys. Rev. D* **76**, 064031 (2007), [arXiv:gr-qc/0702072](#) .
- [67] T. Damour, P. Jaranowski, and G. Schafer, *Phys. Rev. D* **78**, 024009 (2008), [arXiv:0803.0915 \[gr-qc\]](#) .
- [68] D. Singh, *Phys. Rev. D* **78**, 104029 (2008), [arXiv:0808.3006 \[gr-qc\]](#) .
- [69] D. Singh, *Phys. Rev. D* **78**, 104028 (2008), [arXiv:0808.3005 \[gr-qc\]](#) .
- [70] E. Harms, G. Lukes-Gerakopoulos, S. Bernuzzi, and A. Nagar, *Phys. Rev. D* **93**, 044015 (2016), [Addendum: *Phys. Rev. D* **100**, 129901 (2019)], [arXiv:1510.05548 \[gr-qc\]](#) .
- [71] S. Mukherjee, *Phys. Rev. D* **97**, 124006 (2018).
- [72] K. Okabayashi and K.-i. Maeda, *PTEP* **2020**, 013E01 (2020), [arXiv:1907.07126 \[gr-qc\]](#) .
- [73] P. Sheoran, H. Nandan, E. Hackmann, U. Nucamendi, and A. Abebe, *Phys. Rev. D* **102**, 064046 (2020), [arXiv:2006.15286 \[gr-qc\]](#) .
- [74] F. Atamurotov, S. Shaymatov, P. Sheoran, and S. Siwach, *Journal of Cosmology and Astroparticle Physics* **2021**, 045 (2021).
- [75] M. Shahzadi, M. Kološ, Z. Stuchlík, and Y. Habib, (2021), [arXiv:2104.09640 \[astro-ph.HE\]](#) .
- [76] N. Warburton and L. Barack, *Phys. Rev. D* **83**, 124038 (2011), [arXiv:1103.0287 \[gr-qc\]](#) .
- [77] S. Isoyama, L. Barack, S. R. Dolan, A. Le Tiec, H. Nakano, A. G. Shah, T. Tanaka, and N. Warburton, *Phys. Rev. Lett.* **113**, 161101 (2014), [arXiv:1404.6133 \[gr-qc\]](#) .
- [78] M. van de Meent, *Phys. Rev. Lett.* **118**, 011101 (2017), [arXiv:1610.03497 \[gr-qc\]](#) .
- [79] A. J. Hanson and T. Regge, *Annals Phys.* **87**, 498 (1974).
- [80] R. M. Wald, *Phys. Rev. D* **6**, 406 (1972).
- [81] A. A. Deriglazov and W. Guzmán Ramírez, *Adv. Math. Phys.* **2017**, 7397159 (2017), [arXiv:1710.07135 \[gr-qc\]](#) .
- [82] A. A. Deriglazov and W. Guzmán Ramírez, *Phys. Lett. B* **779**, 210 (2018), [arXiv:1802.08079 \[gr-qc\]](#) .
- [83] M. Kamata and M. Kasuya, *Phys. Lett. B* **103**, 351 (1981).
- [84] M. Mathisson, *Acta Phys. Polon.* **6**, 163 (1937).
- [85] A. Papapetrou, *Proc. Roy. Soc. Lond. A* **209**, 248 (1951).
- [86] S. A. Hojman, *Electromagnetic and Gravitational Interactions of a Spherical Relativistic Top*, Ph.D. thesis, Princeton University, 1975 (unpublished).
- [87] R. Hojman and S. Hojman, *Phys. Rev. D* **15**, 2724 (1977).
- [88] S. A. Hojman and F. A. Asenjo, *Class. Quant. Grav.* **30**, 025008 (2013), [arXiv:1203.5008 \[physics.gen-ph\]](#) .
- [89] C. W. Misner, K. S. Thorne, and J. A. Wheeler, *Gravitation* (W. H. Freeman, San Francisco, 1973).
- [90] S. L. Shapiro and S. A. Teukolsky, *Black Holes, White Dwarfs, and Neutron Stars* (John Wiley & Sons, New York, 1983).
- [91] E. Corinaldesi and A. Papapetrou, *Proc. Roy. Soc. Lond. A* **209**, 259 (1951).
- [92] C. Armaza, M. Bañados, and B. Koch, *Class. Quant. Grav.* **33**, 105014 (2016), [arXiv:1510.01223 \[gr-qc\]](#) .
- [93] N. Zalaquett, S. A. Hojman, and F. A. Asenjo, *Class. Quant. Grav.* **31**, 085011 (2014), [arXiv:1308.4435 \[gr-qc\]](#) .
- [94] L. D. Landau and E. M. Lifshitz, *The Classical Theory of Fields*, Landau (Butterworth-Heinemann, San Francisco, 1987) p. 402.
- [95] C. Møller, *Commun. Dublin Inst. Advan. Stud.* **A5** (1949).
- [96] R. Wald, *Phys. Rev. D* **6**, 406 (1972).
- [97] M. Saijo, K.-i. Maeda, M. Shibata, and Y. Mino, *Phys. Rev. D* **58**, 064005 (1998).
- [98] W. Tulczyjew, *Acta Phys. Polon.* **18**, 393 (1959).
- [99] A. H. Taub, *Physical Review* **74**, 328 (1948).
- [100] W. G. Dixon, *Riv. Nuovo Cimento Soc. Ital. Fis.* **34**, 317 (1964).
- [101] L. F. O. Costa and J. Natário, *Fund. Theor. Phys.* **179**,

215 (2015), [arXiv:1410.6443 \[gr-qc\]](#) .

- [102] R. Schattner, *Gen. Rel. Grav.* **10**, 395 (1979).
- [103] We work with the z component of total angular momentum, orbital angular momentum, and spin (i.e., J_z, L_z

and S_z) throughout the paper, but we drop the subscript z everywhere for simplicity only.